Original Article

CAMBRIDGE
UNIVERSITY PRESS

A geochemical and biostratigraphic approach to investigating regional changes in sandstone composition through time; an example from Paleocene–Eocene strata, Taranaki Basin, New Zealand

Karen E. Higgs[1] , Stuart Munday[2], Anne Forbes[2], Erica M. Crouch[1] and Matthew W. Sagar[1]

[1]GNS Science, 1 Fairway Drive, Avalon, Lower Hutt, New Zealand and [2]Chemostrat Australia Pty. Ltd, 1131 Hay Street, West Perth, WA 6005, Australia

Abstract

A geochemical and biostratigraphic approach has been applied to investigate the spatial and stratigraphic variability of Palaeogene sandstones from key wells in Taranaki Basin, New Zealand. Chronostratigraphic control is predominantly based on miospore zonation, while differences in the composition of Paleocene and Eocene sandstones are supported by geochemical evidence. Stratigraphic changes are manifested by a significant decrease in Na_2O across the New Zealand miospore PM3b/MH1 early Eocene zonal boundary, at approximately 53.5 Ma. The change in Na_2O is associated with a decrease in baseline concentrations of many other major (MnO, CaO, TiO_2) and trace elements, and is interpreted to reflect a significant change in sandstone maturity. Paleocene sandstones are characterized by abundant plagioclase (albite and locally Na–Ca plagioclase), significant biotite and a range of heavy minerals, while Eocene sandstones are typically quartzose, with K-feldspar dominant over plagioclase, low mica contents and rare heavy minerals comprising a resistant suite. This change could reflect a change in provenance from local plutonic basement during the Paleocene Epoch to relatively quartz- and K-feldspar-rich granitic sources during Eocene time. However, significant quartz enrichment of Eocene sediment was also likely due to transportation reworking/winnowing along the palaeoshoreface and enhanced chemical weathering, driven in part by long-term global warming associated with the Early Eocene Climatic Optimum. The broad-ranging changes in major-element composition overprint local variations in sediment provenance, which are only detectable from the immobile trace-element geochemistry.

1. Introduction

Detrital sandstone composition is a key primary control for reservoir quality, and understanding regional and stratigraphic variability in composition can aid reservoir quality prediction. Typically, mineralogically mature, quartzose sandstones have a higher potential for good reservoir properties compared with feldspathic and/or lithic sandstones (e.g. Bloch, 1994; Worden *et al.* 2000; Tobin & Schwarzer, 2014). Sediment provenance is one of the main factors controlling the quartz–feldspar–lithic (QFL) composition. However, the original provenance signature may be overprinted or altered through the sediment-transport history and post-depositional alteration (Morton & Hallsworth, 1999). In recent years, inorganic geochemistry has been increasingly used to determine the mineralogy and provenance of sedimentary successions (e.g. Wright *et al.* 2010; Ikhane *et al.* 2014), and can be particularly useful in regions where there is little or no core available for more traditional petrographic studies.

Bulk-rock geochemistry, primarily from cuttings samples, has been used in this study to investigate compositional changes through time in Paleocene–Eocene strata of Taranaki Basin, New Zealand. The deposits comprise a range of quartz arenites, subfeldsarenites and feldsarenites (classification according to Folk *et al.* 1970), and are therefore characterized by highly variable feldspar abundance and type (e.g. Higgs & King, 2018). Previous petrographic studies suggest an increase in sandstone maturity from lower to middle Palaeogene strata (e.g. Higgs, 2002, 2010, 2013; Higgs & King, 2018), with highly mature quartz arenites being a particular feature of all Eocene strata in New Zealand (e.g. Bernet & Bassett, 2016). The primary goal of this study was to investigate the use of downhole bulk-rock geochemical data to illustrate compositional changes from relatively feldspathic to relatively quartzose sandstones. Strata were analysed from a few, widely spaced wells (mostly > 40 km spacing) and constrained by a robust biostratigraphic framework in order to interpret regional trends in geochemistry and

composition with respect to time and to changes in palaeoclimate. Results demonstrate how geochemical data can be used in stratigraphic and provenance studies and, in particular, how they might provide valuable insights into the geological understanding of areas that have limited datasets and few cored sections. Ultimately, this has implications both for predicting reservoir potential and as an analogue for ongoing climate change (Zeebe *et al.* 2016; Forster *et al.* 2020).

2. Geological setting

2.a. Study area and basin history

The Taranaki Basin is located predominantly offshore to the west of New Zealand's North Island (Fig. 1), and forms one of a series of connected Cretaceous–Cenozoic basins that extend along western New Zealand (King *et al.* 1999). Basin development was associated with the break-up of the eastern margin of Gondwana and formation of the Tasman Sea (Thrasher, 1990; Bal, 1994; King & Thrasher, 1996; King *et al.* 1999; Strogen *et al.* 2017). Extensional faulting began during Late Cretaceous time with syn-rift depocentres locally persisting into the Paleocene Epoch and a subsequent passive margin represented by a prolonged (*c.* 30 Ma) period of tectonic quiescence (King & Thrasher, 1996; Strogen, 2011). The tectonic regime started to change during late Eocene time in response to the development of a new plate boundary zone (Stagpoole & Nicol, 2008; Strogen *et al.* 2014); from early Miocene time, the eastern and southern parts of the Taranaki Basin were dominated by convergent margin-related tectonics (King & Thrasher, 1992; Bull *et al.* 2019).

2.b. Palaeogene stratigraphy

Terrestrial to shallow-marine Palaeogene strata are subdivided by age and lithology into four formations that are thought to represent major second- to third-order depositional sequences (King & Thrasher, 1996): (1) Paleocene–lowermost Eocene Farewell Formation; (2) lower–middle Eocene Kaimiro Formation; (3) middle–upper Eocene Mangahewa Formation; and (4) uppermost Eocene McKee Formation, with distal time-equivalent facies to these strata mostly represented by the marine Turi Formation (Fig. 2). These lower–middle Palaeogene strata form the focus of the current study. Upper Palaeogene strata comprise outer shelf to upper bathyal clastics and carbonates that were deposited following abrupt tectonically induced subsidence during latest early Oligocene time (King & Thrasher, 1996), and are not included in the current study.

Palaeogene strata and stage boundaries in New Zealand are based primarily on benthic and planktic foraminifera (Hornibrook *et al.* 1989; Morgans *et al.* 2004), with stages correlated with the International Geologic Time Scale (Gradstein *et al.* 2012) following Raine *et al.* (2015) (Fig. 2). However, the Paleocene–Eocene reservoir fairway is dominated by coastal to shallow-marine deposits, and calcareous microfossils (e.g. foraminifera) are rare. Miospore (spore and pollen) assemblages are typically well preserved in these facies and can provide robust age control using the zonal scheme of Raine (1984; revised in Raine, 2004) (Fig. 2).

2.c. Basement geology

Cambrian–Early Cretaceous basement rocks of New Zealand have been subdivided by Landis & Coombs (1967) into Western and Eastern provinces. The former record early Palaeozoic terrane

accretion and plutonism along the eastern Gondwana margin (Cooper, 1989; Tulloch *et al.* 2009), while the latter represents Mesozoic accretion to the supercontinent (Coombs *et al.* 1976; Howell, 1980; Bradshaw, 1989).

The Western Province is considered to have been the main sediment source for Palaeogene strata in Taranaki Basin (Hill & Collen, 1978; Smale & Morton, 1987; Smale, 1992, 1996; Kamp, 2012; Higgs & King, 2018). It comprises the metasedimentary Takaka and Buller terranes (Cooper, 1989), which are intruded by a series of Devonian–middle Cretaceous batholiths/intrusives (Coombs *et al.* 1976; Howell, 1980; Tulloch, 1988; Bradshaw, 1989; Mortimer, 2004; Mortimer *et al.* 2014; Tulloch *et al.* 2019). Overall, the Buller Terrane comprises mineralogically mature, quartzose sandstones, while the Takaka Terrane comprises a much wider range of lithologies, including volcanics, volcanoclastic sandstones and carbonates (Cooper, 1989). Plutonic rocks predominantly occur within two large batholiths, known as the Karamea and Median batholiths, but they also form smaller isolated plutons and batholiths throughout the Western Province (Tulloch, 1983, 1988). These rocks are collectively named the Tuhua Intrusives by Mortimer *et al.* (2014) and comprise several geochemical suites.

3. Methodology

Six study wells were selected for analysis along the Paleocene–Eocene reservoir fairway (Fig. 1), with a total of 458 geochemical analyses undertaken on Cretaceous–Palaeogene sediments and a few basement samples (Table 1). Most samples are from uncored sections, with samples taken from washed ditch cuttings at *c.* 20 m sampling intervals. A closer sampling interval of 3 m and 5 m was undertaken at Kupe South-4 for core and uncored intervals, respectively. Samples were collected from the New Zealand Petroleum and Minerals (NZP&M) National Core Store, and boreholes are close to vertical with depths or thicknesses quoted in metres (measured depth below Kelly bushing or bkb).

Cutting samples were sieved to obtain the representative lithology, and obvious contamination was removed using a binocular microscope (e.g. mud additives, drill bit contamination, cavings). The samples were ground in agate and sample powders prepared by the alkali fusion procedure of Jarvis & Jarvis (1992a, b). Major elements were analysed by inductively coupled plasma-optical emission spectrometry (ICP-OES) and trace elements by inductively coupled plasma-mass spectrometry (ICP-MS), with quantitative data acquired for 50 elements (see online Supplementary Material S1; http://journals.cambridge.org/geo). Precision errors are *c.* 2% for the major element data, *c.* 3% for the high-abundance trace-element data and *c.* 5% for most rare Earth elements (REE). All analyses were conducted at Chemostrat Ltd (UK).

Cuttings samples were assessed for potential caving and contamination by comparing chemically derived gamma-ray (Chem-GR) with wireline gamma-ray; the full suite of geochemical and Chem-GR data are provided in online Supplementary Material S1 and S2 (available at http://journals.cambridge.org/geo). Contamination issues were assessed by comparing the relative abundance of Ba and S, both of which are common drilling fluid additives. Cross-plots suggest that contamination is low in most samples, but has been identified in two wells (Turangi-3 and Kowhai-1A). The trace element Eu also shows a positive correlation with Ba at these two wells, which may reflect the interference of different Ba and Eu isotope peaks on the ICP-MS spectrum arising from drilling fluid contamination, and which was not corrected for at the time of analysis. Based on this
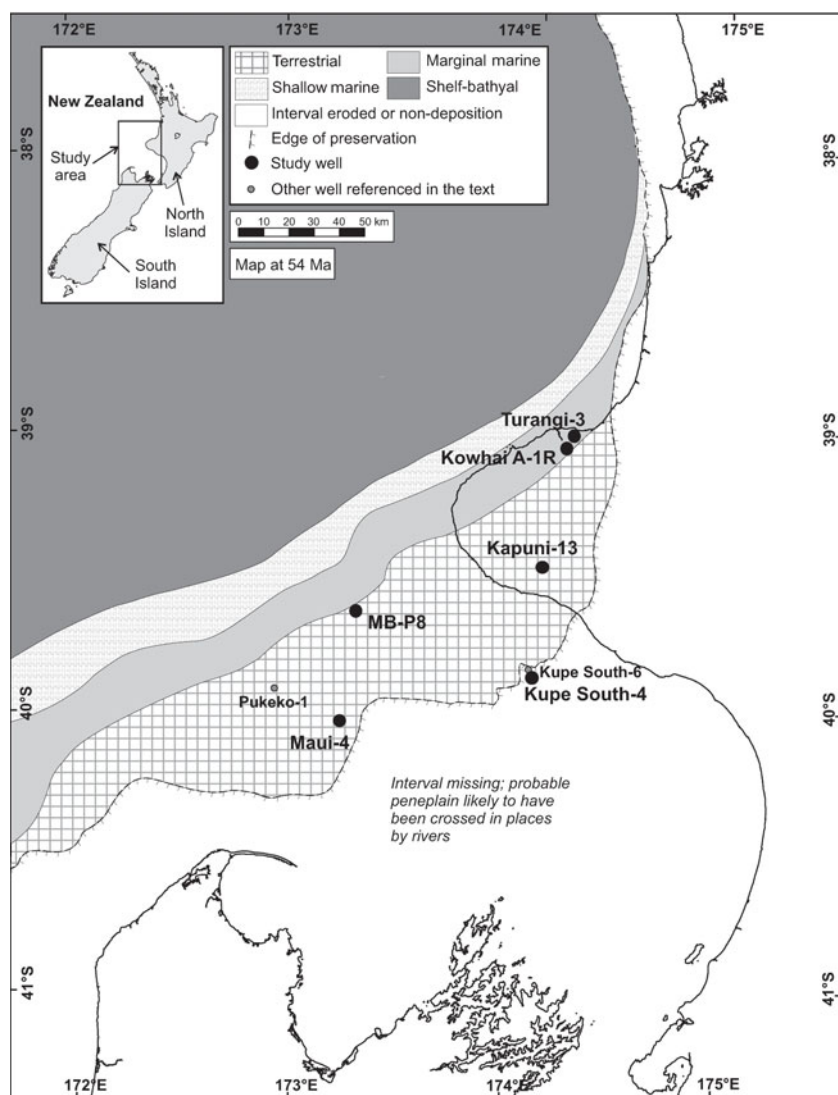
Fig. 1. Taranaki Basin map showing study wells. Palaeogeography at 54 Ma shows the orientation of the middle Eocene palaeoshoreline and general position of facies belts for lower Eocene strata (after Strogen 2011). The present-day shoreline of the Taranaki Peninsula and latitude and longitude are also shown; see inset for location of the study area.

information, the Ba, S and Eu data were excluded from interpretations at Turangi-3 and Kowhai-1A.

Heavy mineral analysis was undertaken on the 40–250 μm fractions of five samples from Kupe South-4 and a further four samples from offset well Kupe South-6. Heavy mineral grains were separated in a sodium heteropolytungstate solution (LST Fastfloat, 2.89 g cm^{-3}) using the funnel separation technique (Mange & Maurer, 1992), and a representative portion of heavy mineral grains taken using a micro-splitter. The grains were mounted on a glass slide in Canada Balsam (refractive index (RI) of 1.55), and point-counted using a Nikon Eclipse polarizing microscope.

A well-constrained chronostratigraphic framework was developed for the six study wells using available palynology and foraminifera data (Raine, 1984; Bartram *et al.* 1996; Higgs *et al.* 2006; Crouch, 2010; Raine & Mildenhall, 2011; Crampton *et al.* 2012; Crouch & Raine, 2012; Raine & Schiøler, 2012). In addition, geochemical results were integrated with published thin-section, x-ray diffraction (XRD) QEMSCAN®, trace-element geochemistry and U–Pb zircon geochronology data from relevant reservoir sandstones (Clews & Soo, 1994; Higgs, 2010; Higgs *et al.* 2012b; Adams *et al.* 2017) and volumetrically significant

Devonian–middle Cretaceous granitoids (references provided in online Supplementary Material S3, available at http://journals. cambridge.org/geo). Alteration indices were used as one method to evaluate possible zones of enhanced chemical weathering through the Palaeogene interval and have been calculated from molecular proportions using chemical index of weathering (CIW; Harnois, 1988), plagioclase index of alteration (PIA; Fedo *et al.* 1995) and chemical proxy of alteration (CPA; Buggle *et al.* 2011).

4. Results and interpretation

4.a. Chronostratigraphic framework

Paleocene strata include the Farewell Formation (sandstones) and Turi Formation (mudstones) and are correlated with the PM3a miospore zone, and/or are assigned a Teurian (Dt = Danian–Thanetian) age from foraminiferal assemblages (Fig. 2). They are present in all study wells, with the thickest Paleocene intervals sampled for geochemical analysis in wells Kupe South-4 and Maui-4 (thicknesses of > 500 m and 400 m, respectively). Only the uppermost Paleocene strata have been analysed in

Table 1. Bulk-rock geochemistry samples from six wells, Taranaki Basin

| Well	Interval (m)	Stratigraphy	Sample type	*n*
Kapuni-13	3240–4222	Uppermost Paleocene – upper Eocene	Cuttings	48
Kowhai-A1	4441–5461	Uppermost Paleocene – middle Eocene	Cuttings	52
Kupe South-4	3052.5–3798	Upper Cretaceous – lowermost Eocene	Core and cuttings	149
Maui B-P8	2800–3710	Basement and overlying uppermost Paleocene – upper Eocene	Cuttings	44
Maui-4	3822–3917	Basement	Cuttings	65
	2005–2783	Paleocene – upper Eocene		
Turangi-3	3426–5401	?Uppermost Paleocene – upper Eocene	Cuttings	100
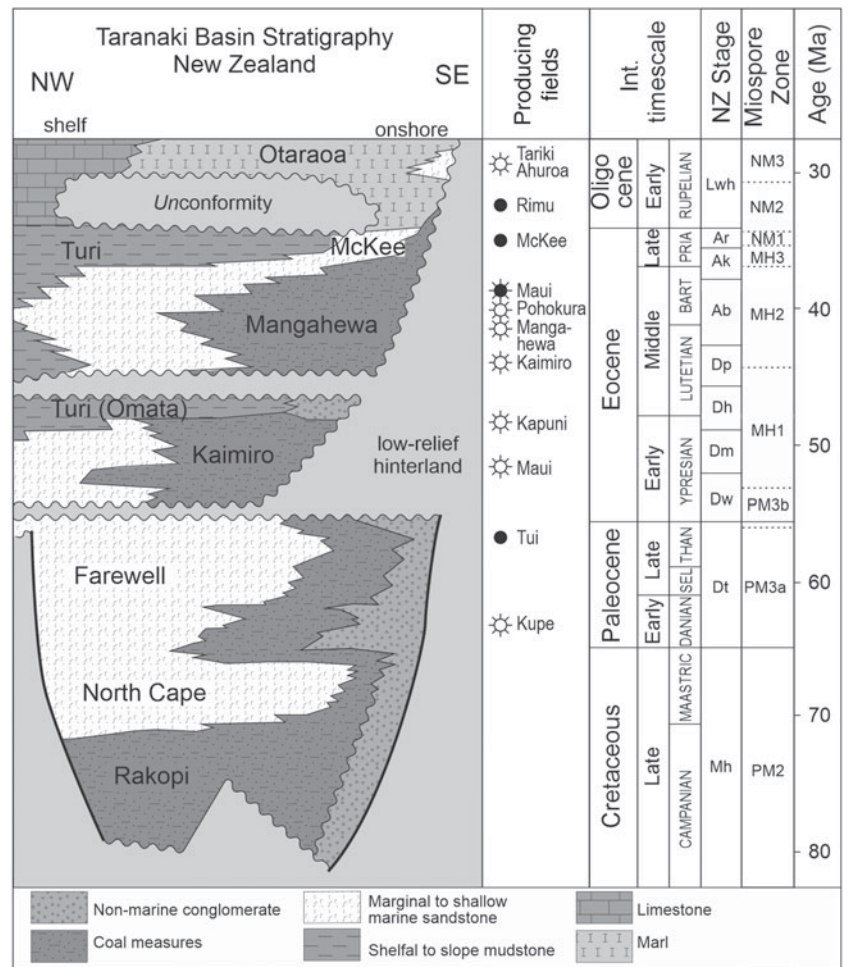
Fig. 2. Cretaceous and Palaeogene stratigraphic framework for the Taranaki Basin, New Zealand, plotted against the geological timescale and correlative miospore zones. The stratigraphic framework is modified from King & Thrasher (1996), international timescale from Gradstein *et al.* (2012) and miospore zones from Raine (1984, 2004). Dt – Teurian; Dw – Waipawan; Dm – Mangaorapan; Dh – Heretaungan; Dp – Porangan; Ab – Bortonian; Ak – Kaiatan; Ar – Runangan; Lwh – Whaingaroan.

other wells. For the purposes of this study, the Paleocene/Eocene (P/E) boundary is approximately correlated with the PM3a/PM3b miospore zonal boundary, although the P/E boundary is thought to occur slightly above this, within the lowermost part of the PM3b miospore zone (Ian Raine, pers. comm., 2018) (Fig. 2). Biostratigraphic data suggest that the P/E boundary has been penetrated in all six study wells, and sampling for geochemical analysis extends across the boundary in all cases (Fig. 3).

The earliest Eocene PM3b miospore zone represents a relatively short time interval (*c.* 2.5 Ma; Fig. 2) and is correlated with the lowermost Kaimiro Formation (sandstone) and time-equivalent

Turi Formation (mudstones). The PM3b zone is relatively well constrained in four study wells where it reaches up to *c.* 170 m in thickness (Fig. 3). In Turangi-3, zone PM3b is not confidently identified, although it is assumed to be present based on similar log profiles within nearby well Kowhai A-1R. A discrete PM3b zone has not been identified in the more proximal well Maui-4; if present, it is likely to be a very thin or condensed interval (< 80 m thick PM3a/PM3b zone). A thin or absent zone has previously been recognized in lower Eocene coastal plain settings such as Pukeko-1 (cf. Fig. 1), where it is interpreted to be associated with significant fluvial incision (Higgs *et al.* 2017). A very thin
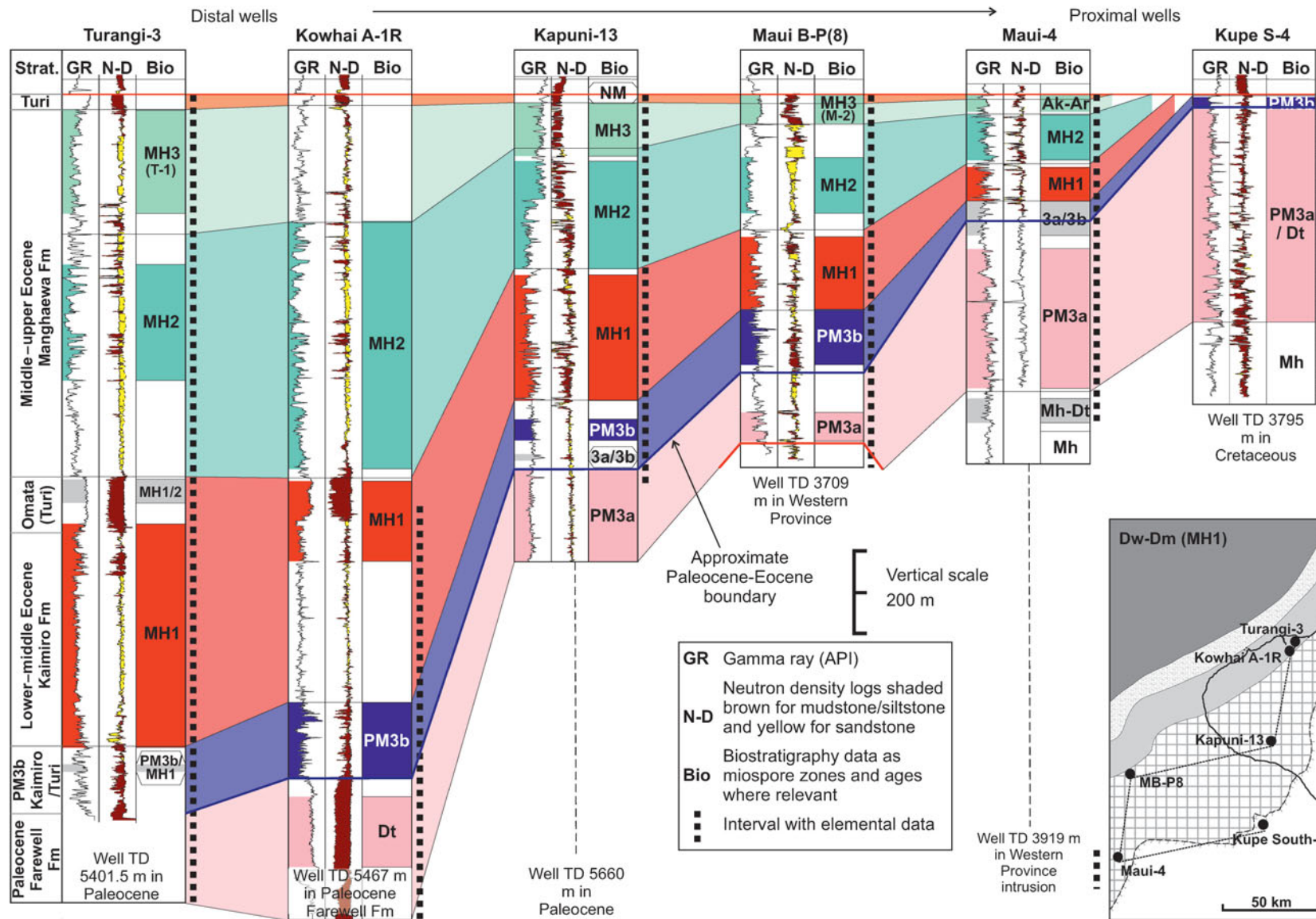
Fig. 3. (Colour online) Cross-section showing chronostratigraphic framework for the study wells; location of the transect is shown on the inset map, with legends on Figures 1 and 2 for facies belts and biostratigraphic data, respectively. Intervals sampled for geochemical analyses are indicated; mudstone/siltstone intervals are indicated by brown shading on the neutron-density (N-D) log crossover.

PM3b zone also occurs in Kupe South-4 (*c.* 30 m; Fig. 3) where it represents the only record of Eocene strata, unconformably overlain by Oligocene mudstones.

Most lower–middle Eocene strata in the Taranaki Basin are correlated with the MH1 miospore zone, which ranges in age from late Waipawan to early Porangan (lDw–eDp = Ypresian–Lutetian, *c.* 10 Ma duration; Fig. 2). The PM3b/MH1 zonal boundary has been cored at MB-P(8), where it is very sharp and possibly indicates a sequence boundary (Higgs *et al.* 2017; Ian Raine, pers. comm., 2017). The MH1 zone is recognized in five of the study wells (absent from Kupe South-4) and corresponds to the main Kaimiro Formation reservoir. The MH1 zone is thickest in the most distal wells (> 500 m thickness at Turangi-3), thinning towards the more proximal Maui-4 well (< 100 m thickness; Fig. 3).

Regional marine transgression is recognized in the lower part of middle Eocene strata (Porangan Stage) at the MH1/MH2 zonal boundary, which resulted in deposition of the Omata Member and equivalent strata (Higgs *et al.* 2012*a*) (Figs 2, 3). The MH1/MH2 zonal boundary is well constrained in four study wells, inferred in Turangi-3 based on log correlation with Kowhai A-1R, and absent from Kupe South-4. The overlying MH2 miospore zone ranges in age from Porangan to early Kaiatan (Dp–eAk = Lutetian–Bartonian, *c.* 6 Ma duration; Fig. 2), and is correlated with the main Mangahewa Formation reservoir. A similar thinning pattern is observed in zone MH2, as is seen in the MH1 zone, with the thickest interval in the most distal wells (*c.* 600 m at Turangi-3 and Kowhai A-1R) and thinning in the most proximal well Maui-4 (*c.* 110 m). Sampling for geochemical analyses was not undertaken in the MH2 zone at Kowhai A-1R but was continuous to the top Eocene section in all other study wells (Fig. 3).

Miospore zones MH3 and NM1 are representative of uppermost Eocene strata, ranging in age from Kaiatan to Runangan (Ak–Ar = Bartonian–Priabonian, *c.* 3 Ma duration), and the zones are correlated with parts of the Mangahewa, McKee and Turi formations (Fig. 2). Chronostratigraphic control at this level is available for Kapuni-13 and Maui-4, with biostratigraphic data from offset wells Turangi-1 and Maui-2 used as a guide to uppermost Eocene correlation in wells Turangi-3 and MB-P(8), respectively. Despite the relatively short time interval for these zones, the MH3 interval is relatively thick in the distal wells (> 250 m at Turangi-1), and thinner (<100 m) in wells further west (MB-P(8) and Maui-4; Fig. 3).

The Paleocene–Eocene section forms the main focus of this paper. However, geochemical sampling was undertaken on older deposits in three wells. Upper Cretaceous strata, which are dated by miospore (zone PM2) and foraminiferal assemblages (Haumurian, Mh; Fig. 2), have been penetrated in two study wells. Geochemical sampling was undertaken in the uppermost part of Cretaceous strata in Maui-4 and through the entire penetrated Cretaceous interval in Kupe South-4 (Fig. 3). In addition, two wells penetrate igneous basement (Maui-4 and MB-P(8)) and bulk-rock geochemical data was acquired through both basement intervals to aid provenance discrimination.

4.b. Maui-4 and MB-P(8) basement correlation

Granite basement samples from MB-P(8) show a discrete and relatively mafic composition compared with samples from Maui-4 (SiO_2, 52–55 v. 65–72 wt%; Cr, 92–120 v. 4–11 ppm; Ni, 40–43 v, 0.3–2.4 ppm; TiO_2, 1.01–1.14 v. 0.18–0.49 wt%; e.g. Fig. 4a, b). Petrographic analysis has not been undertaken on these cuttings samples. However, age data from previous work have established

that the granites represent part of the Carboniferous and Cretaceous Median Batholith (U–Pb zircon ages of *c.* 328 Ma at Maui-4 and *c.* 115 Ma at MB-P(8); Tulloch & Mortimer, 2017), with probable age correlation to the Foulwind Suite at Maui-4 (cf. Tulloch *et al.* 2009) and either Separation Point or Rahu suite at MB-P(8) (cf. Tulloch & Kimbrough, 2003). However, there is a significant range in the geochemical composition of all the igneous suites (e.g. Tulloch, 1983; Muir *et al.* 1995, 1998; Tulloch & Kimbrough, 2003; Allibone *et al.* 2009; Tulloch *et al.* 2009), which makes it difficult to confirm these correlations on the basis of their geochemical signature (e.g. Fig. 4). Additionally, basement samples may have undergone different levels of alteration, which can change their geochemistry and thereby make correlations more difficult. Significantly, basement samples from MB-P(8) display very high alteration indices (CIW = 76–90, compared with 48 of average andesite where $SiO_2 = 58$ wt%), which could be indicative of moderate to significant chemical weathering and would be consistent with the well completion description as a basement wash (STOS, 1994). In contrast, Maui-4 basement samples have moderate alteration indices (CIW = 55–60 and $SiO_2 = 65–72$ wt%), which are intermediate between average andesite and rhyolite (CIW = 62 and SiO_2 of 73 wt%) and would be consistent with fresh (unaltered) samples.

Given the above, together with the small number of samples analysed, the basement correlation at Maui-4 and MB-P(8) has been primarily based on the U–Pb zircon ages of Tulloch & Mortimer (2017). Samples from Maui-4 overlap the ranges for most major and trace elements of published data from the Foulwind Suite (Fig. 4c–f), and are therefore consistent with a Foulwind correlation. Samples from MB-P(8) display a geochemical signature that falls outside the typical range of published data from the Separation Point Suite (Fig. 4c–f), but given the high alteration indices it is suggested that these differences could largely be due to the effects of chemical weathering. While the data are equivocal, a Separation Point Suite is favoured over the Rahu Suite for MB-P(8) basement based on (a) the mafic composition, which has a much lower SiO_2 content than all known samples from the Rahu Suite, and (b) the location of MB-P(8), which is further east than known occurrences of the Rahu Suite.

4.c. Mineral affinities of elements, Palaeogene sandstones

Bulk-rock geochemical data from lower–middle Palaeogene sandstones have been compared with available petrographic data to establish element–mineral affinities. Interpretations are primarily based on data from well MB-P(8), which has a long (*c.* 190 m) Eocene cored interval, and well Kupe South-4, which has a shorter (*c.* 66 m), dominantly Paleocene, cored interval. The element–mineral affinities determined from petrographic data are confirmed by bivariate relationships observed for sandstone lithologies from the full geochemical dataset (plots presented in online Supplementary Material S4, available at http://journals.cambridge.org/geo). A summary of the key elements and ratios that have been used in this study to characterize the lithology and sandstone composition are presented in Table 2. Other trends observed between high-field-strength elements are mostly attributed to heavy mineral composition, and are discussed further in Section 4.g.

4.c.1. Eocene sandstones, MB-P(8)
Lower Eocene sandstone core from MB-P(8) is described by Clews & Soo (1994) as having a quartzo-feldspathic composition and
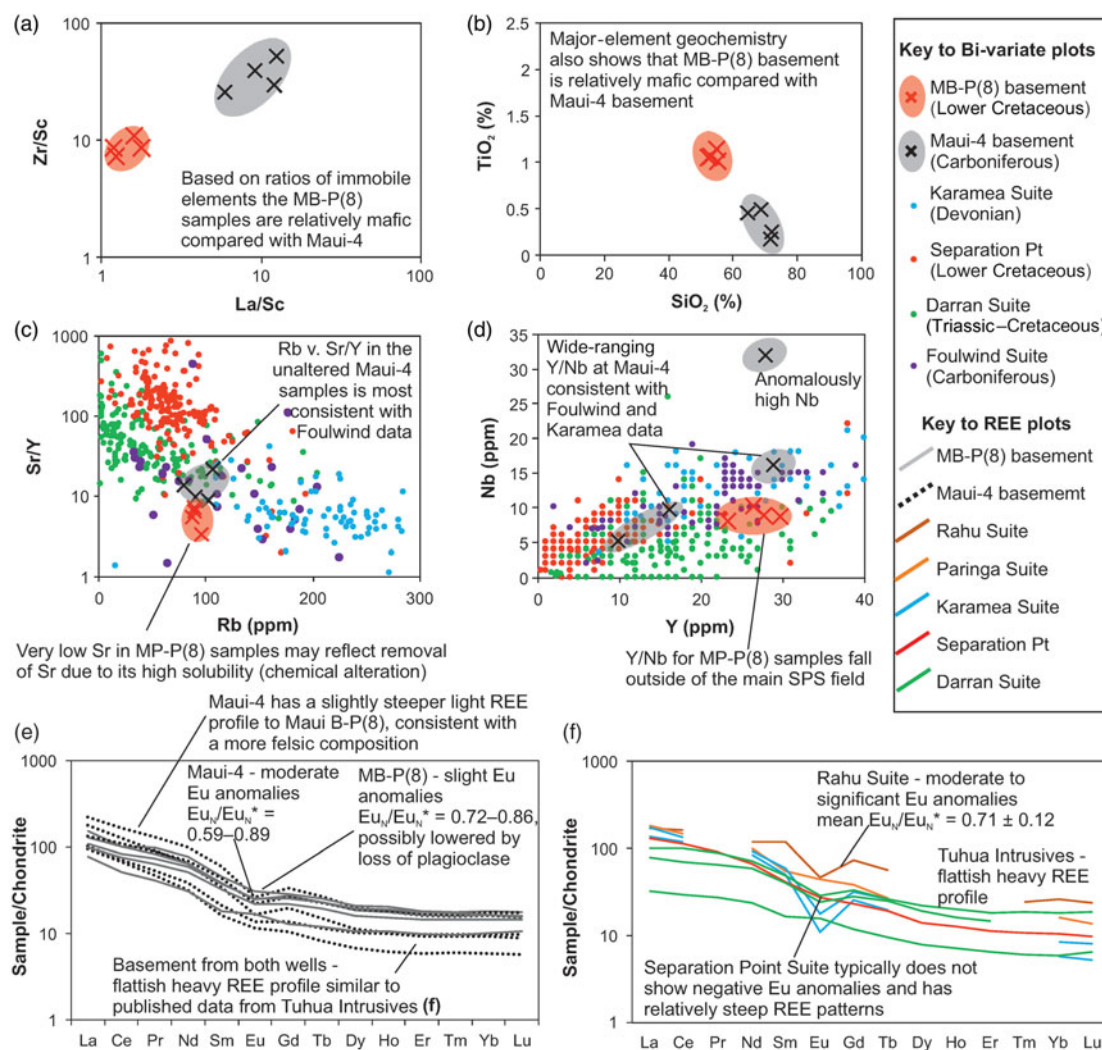
Fig. 4. (Colour online) Geochemical plots for basement samples from Maui-4 and MB-P(8) showing: (a) La/Sc v. Zr/Sc; (b) SiO_2 v. TiO_2; (c) Rb v. Sr/Y; and (d) Y v. Nb. (c, d) Plotted with published geochemical data from selected igneous suites; references provided in online Supplementary Material S3. These trace elements and ratios are some of the best discriminators (e.g. Tulloch & Kimbrough, 2003) but still illustrate the wide variability in suite composition. (e, f) Chondrite-normalized rare Earth element (REE) patterns comparing (e) basement samples from Maui-4 and MB-P(8), and (f) selected published data from McCulloch *et al.* (1987), Muir *et al.* (1996), Waight *et al.* (1998), Price *et al.* (2011) and Sagar *et al.* (2016).

comprising fine-grained through to coarse-grained, granular sub-arkose and arkose. Other grains have been described as trace to minor rock fragments (mostly plutonic) and trace to abundant accessories (mostly biotite mica with only rare heavy minerals).

Reasonably close matches are observed between the downhole profiles of certain elements (this study) and minerals (Clews & Soo, 1994), despite differences in sample depths and sample type between the XRD and geochemistry samples (core and cuttings, respectively). These relationships support probable element–mineral affinities for SiO_2 and quartz, K_2O and K-feldspar, and Na_2O and plagioclase (Fig. 5); CaO values are very low, which indicates that plagioclase is dominantly albite (Na rich). Clay-fraction XRD data from MB-P(8) (Clews & Soo, 1994) show that illite/mica (K_2O rich) and smectite (Na_2O/CaO rich) are rare or absent in most of the sandstone samples. Only the argillaceous sandstones are reported to contain minor illite; in these lithologies, some of the measured K_2O and associated very high Cs/Rb ratios will be associated with this clay (Fig. 5). Kaolinite, described as authigenic by Clews & Soo (1994), is the dominant clay mineral within the MB-P(8) sandstones. However, only a moderate

relationship is observed between total clay (measured from XRD) and Al_2O_3, which is interpreted to be due to the association of Al_2O_3 with both feldspar and clay minerals (mostly kaolinite).

Whole-rock XRD data demonstrate the patchy distribution of carbonate cements in cored sandstone samples. Calcite is a relatively rare carbonate cement in the petrographic samples (Clews & Soo, 1994), which is consistent with low CaO. Siderite and dolomite are more common, occurring predominantly in the upper cored section (Fig. 5) where they are represented by coincident peaks of MgO, Fe_2O_3 and MnO. However, coincident peaks of MgO, Fe_2O_3 and MnO are also recognized in the lower cored section where siderite and ferroan dolomite have typically not been identified. Based on XRD and thin-section observations, other Fe-rich minerals (pyrite, chlorite, biotite) are all more abundant in the lower cored section (Clews & Soo, 1994), and are therefore the likely main mineral affinities at this stratigraphic level.

Heavy minerals have not been identified from XRD and are reported in trace amounts from thin-section; for this reason, heavy minerals cannot be used to establish element–mineral affinities. However, the abundance of heavy rare Earth elements (HREE)

Table 2. Key bulk-rock elemental data, ratios and alteration indices

Element, ratio or index	Use in study
Cs/Rb	Lithology indicator
K_2O/Rb	Lithology indicator (≥ 0.035 implies sandstone); K-feldspar:illite/mica in sandstones
SiO_2/Al_2O_3	Lithology indicator (≥ 4 implies sandstone)
SiO_2	Quartz and other silicates
K_2O	K-feldspar and illite/mica
Na_2O	Na-feldspar (and smectite)
K_2O/Na_2O	K-feldspar:Na-feldspar
MnO	Carbonates, clays and heavy minerals
CaO	Carbonates, clays and Ca-feldspar
Al_2O_3/alkali ratio	Weathering/alteration
CIW	Weathering/alteration
PIA	Weathering/alteration
CPA	Weathering/alteration

CIW – chemical index of weathering (Harnois, 1988); CPA – chemical proxy of alteration (Buggle *et al.* 2011); PIA – plagioclase index of alteration (Fedo *et al.* 1995)

may give an indication of heavy mineral abundance (see online Supplementary Material S4, available at http://journals.cambridge.org/geo), with HREE strongly related to lithology (Fig. 5). Notably, ratios of some high-field-strength elements (HFSEs; e.g. Hf/Sc, Zr/Y, Ta/HREE) are elevated in the sandstones, which implies relative enrichment of zircon and Ti-bearing heavy minerals over more mafic (and labile) heavy minerals. This is consistent with the few identified heavy minerals reported from thin-section (opaques, limonite and zircon, and rare garnet and tourmaline; Clews & Soo, 1994).

4.c.2. Paleocene–Eocene sandstones, Kupe South-4

Palaeogene sandstones from core and sidewall core (SWC) at Kupe South-4 have been described by Martin *et al.* (1994) as very fine-grained through to very coarse-grained sandstones, mostly of lithic arkose or feldspathic litharenite composition, where igneous fragments (predominantly quartz–feldspar) are the most abundant lithic grain types. Martin *et al.* (1994) note a downhole reduction in quartz abundance, which is mostly compensated for by an increase in plagioclase feldspar, but is also associated with an increase in biotite and heavy minerals (epidote, sphene).

A comparison of geochemistry and thin-section data show reasonably close matches between the profiles of SiO_2 and quartz, and Na_2O and plagioclase, and a fair match between K_2O and K-feldspar (Fig. 6), providing further evidence for these as probable element–mineral affinities. A very clear break in major-element geochemistry is noted close to the top of Paleocene strata (uppermost zone PM3a) at *c.* 3.1 km depth, where deeper samples are characterized by low SiO_2 and high Na_2O and K_2O values. Mineralogically, these changes reflect the downhole increase in plagioclase relative to quartz reported by Martin *et al.* (1994). Petrographic data indicate that K-feldspar does not appreciably increase with depth, and the higher K_2O observed through most of the Paleocene–Cretaceous section will reflect additional K-rich minerals (e.g. illite/mica). In the shallower well section, total clay content from point count data shows a good match with both Al_2O_3 content and alteration indices. XRD confirms that the clay

fraction is predominantly kaolinite, which has been described by Martin *et al.* (1994) as authigenic, formed from the decomposition of biotite, feldspar and rock fragments. Al_2O_3 content in the upper well section is therefore mostly interpreted to be associated with kaolinite and, to a lesser degree, feldspar. In the lower well section (below *c.* 3.1 km), Al_2O_3 content is relatively constant with no apparent match to point-counted total clay; this is interpreted to be due to an overall greater affinity of Al_2O_3 to plagioclase feldspar.

Mineralogical affinities of the other major elements are more difficult to establish, which probably suggests that they are associated with a variety of clay, carbonate and heavy minerals. The profile shape of CaO bears little resemblance to point-counted carbonate, suggesting that calcite is not a significant component of these deposits. Conversely, in the upper well section (above *c.* 3.1 km), coincident peaks of Fe_2O_3, MnO and, to a lesser extent, MgO display a spikey response with some degree of match to the counted carbonate. Although geochemical and petrographic samples are from different depths, these results are considered sufficiently similar to indicate that Fe_2O_3, MnO and MgO are predominantly associated with carbonates in this upper part of the stratigraphy. Qualitative XRD analysis confirms that siderite is the main carbonate phase, and is relatively common in the upper well section (Martin *et al.* 1994).

A significant shift is observed in the baseline concentration of CaO, MgO, Fe_2O_3 and MnO to overall higher and more consistent values below *c.* 3.12 km. The relatively consistent geochemical response is due, in part, to a change in sample type from core (uppermost section) to cuttings (lower section). However, carbonate has not been recorded from most petrographic samples from the lower well section, suggesting that CaO, MgO, Fe_2O_3 and MnO have other mineral affinities through this interval. QEMSCAN data from Higgs *et al.* (2012b) show that plagioclase in Paleocene sandstones at Kupe South-4 includes a significant component of Na–Ca plagioclase (see Section 4.d.2); this is considered to be the main host for CaO below *c.* 3.12 km. However, qualitative clay fraction XRD data also demonstrate a change in clay mineralogy from the upper kaolinite zone to a thick underlying interval where mixed layer chlorite–smectite is the dominant clay (Martin *et al.* 1994). These clays will account for some of the CaO and Na_2O in the lower well section, while a good match between Fe_2O_3, MgO and relative abundance of chlorite–smectite indicates that these clays are also the main hosts for Fe and Mg (Fig. 6). A greater abundance of biotite and heavy minerals identified from thin-section analysis (Martin *et al.* 1994) can also account for some of the MgO, Fe_2O_3, CaO and MnO, as well as TiO_2 and REE. Overall, HREE values are fairly high through most of the Cretaceous–Eocene section, consistent with relatively common heavy minerals, while similar profiles for HREE, SiO_2 and total point-counted clay again demonstrate a relationship between HREE and lithology. Notably, ratios of some HFSEs imply a stratigraphic change in the heavy mineral suite, consistent with the uphole reduction in epidote and sphene (cf. Martin *et al.* 1994) and indicative of relative zircon and Cr-bearing heavy mineral enrichment (e.g. high Hf/Sc and Zr/Y showing a good match with Ta/HREE, Cr/Ce, Cr/Y and Cr/Th).

4.d. Major-element geochemistry

The established mineral affinities of elements have been used to interpret and compare sandstone composition through lower–middle Palaeogene strata. Key elemental data are presented for well MB-P(8) and summarized for all study wells to illustrate systematic
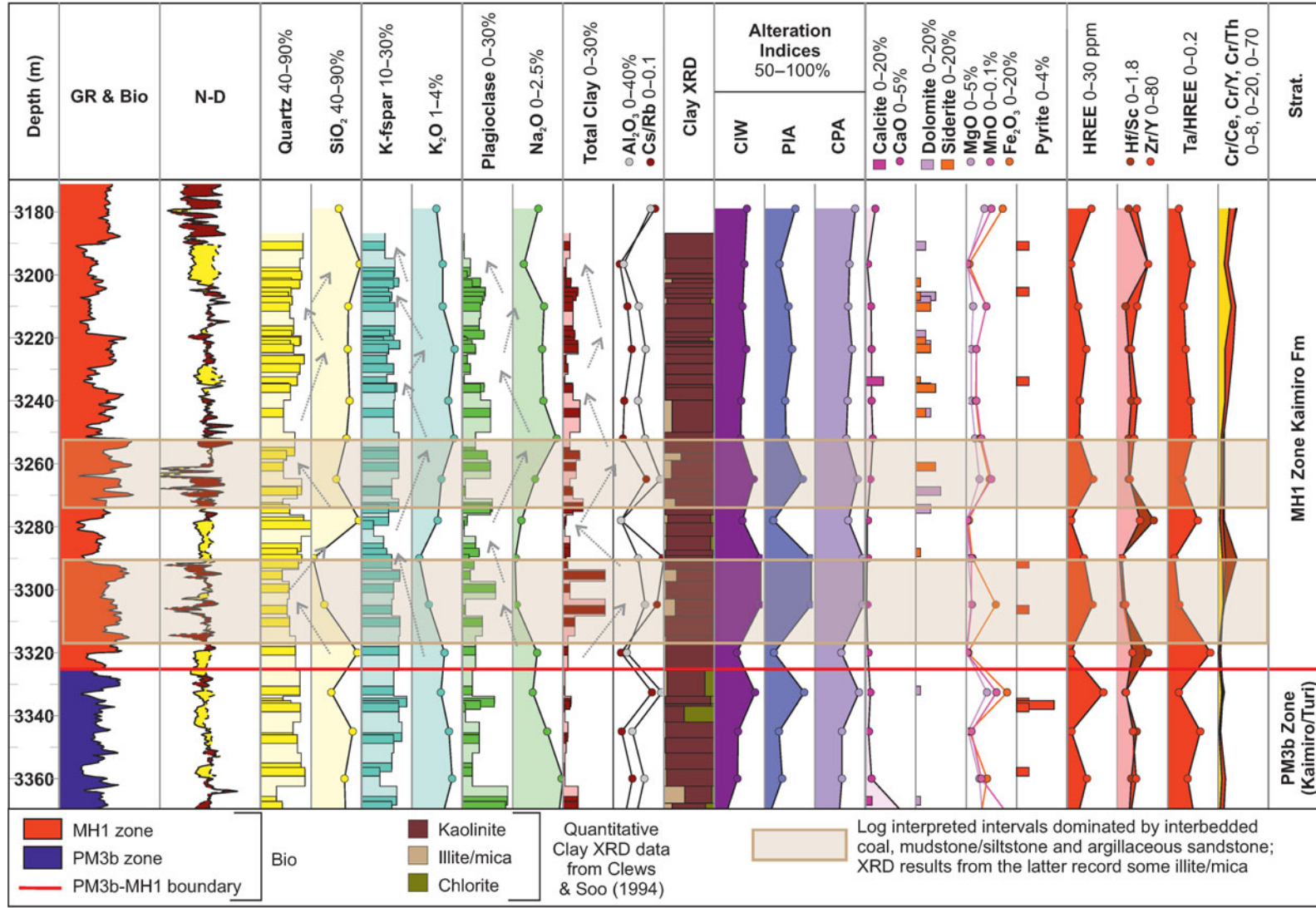
Fig. 5. (Colour online) Comparison of x-ray powder diffraction (XRD) data from core samples (Clews & Soo, 1994) with bulk-rock elemental data from cuttings (this study) plotted against gamma-ray (GR), neutron-density (N-D) and biostratigraphy (Bio) data for well Maui B-P(8). Whole-rock XRD data are plotted as bar charts (dark colour) joined by a bar edge line (pale colour). Elemental data are represented by coloured disks. Mudstone/siltstone intervals are indicated by brown shading on the N-D log crossover. Alteration indices after Harnois (1988), Fedo *et al.* (1995) and Buggle *et al.* (2011).
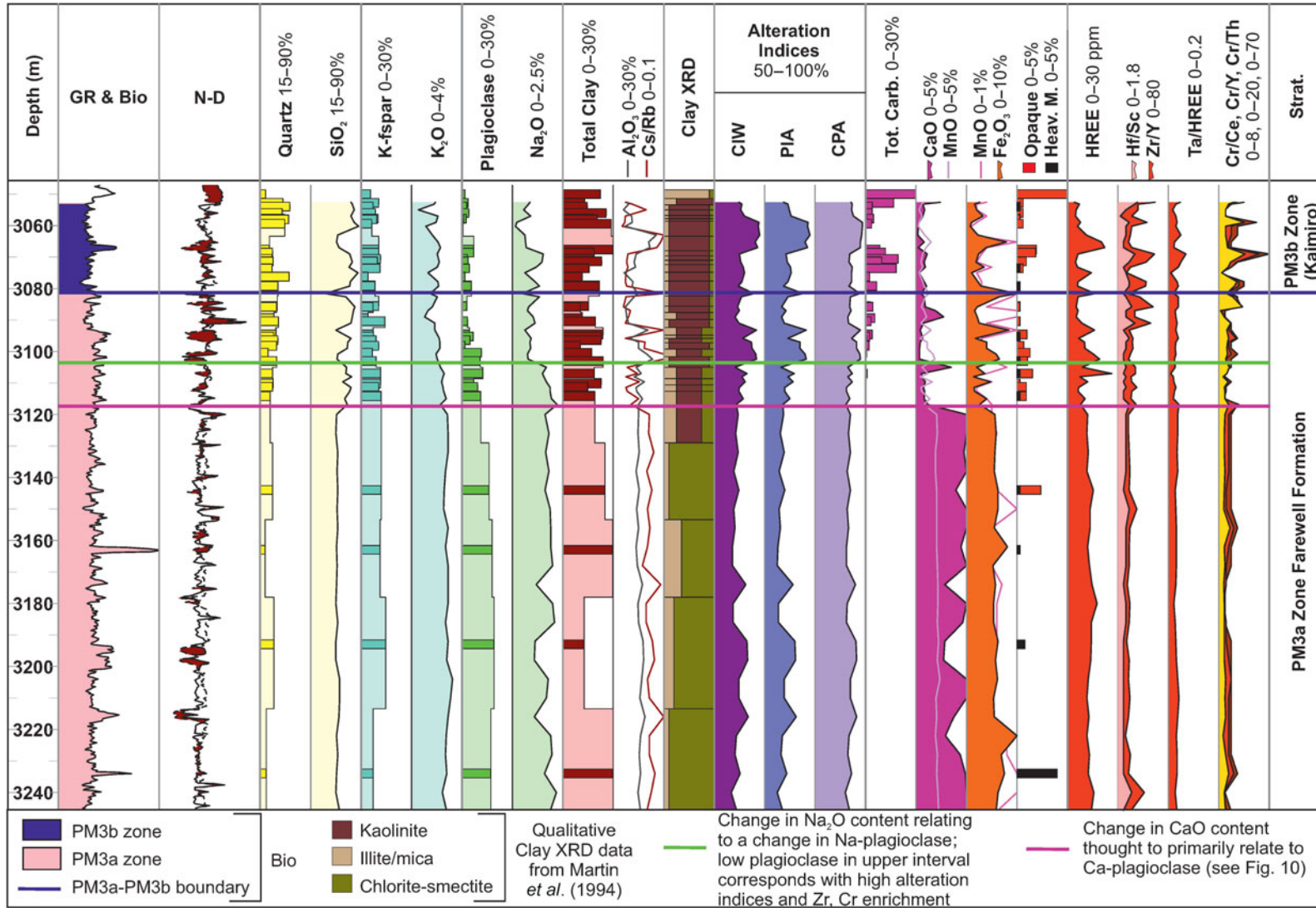
Fig. 6. (Colour online) Comparison of point-count data from core samples (Martin *et al.* 1994) with bulk-rock elemental data from cuttings (this study) plotted against gamma-ray (GR), neutron-density (N-D) and biostratigraphy (Bio) data for well Kupe South-4. Petrographic data are plotted as bar charts (dark colour) joined by a bar edge line (pale colour). Mudstone/siltstone intervals are indicated by brown shading on the N-D log crossover. Alteration indices after Harnois (1988), Fedo *et al.* (1995) and Buggle *et al.* (2011).
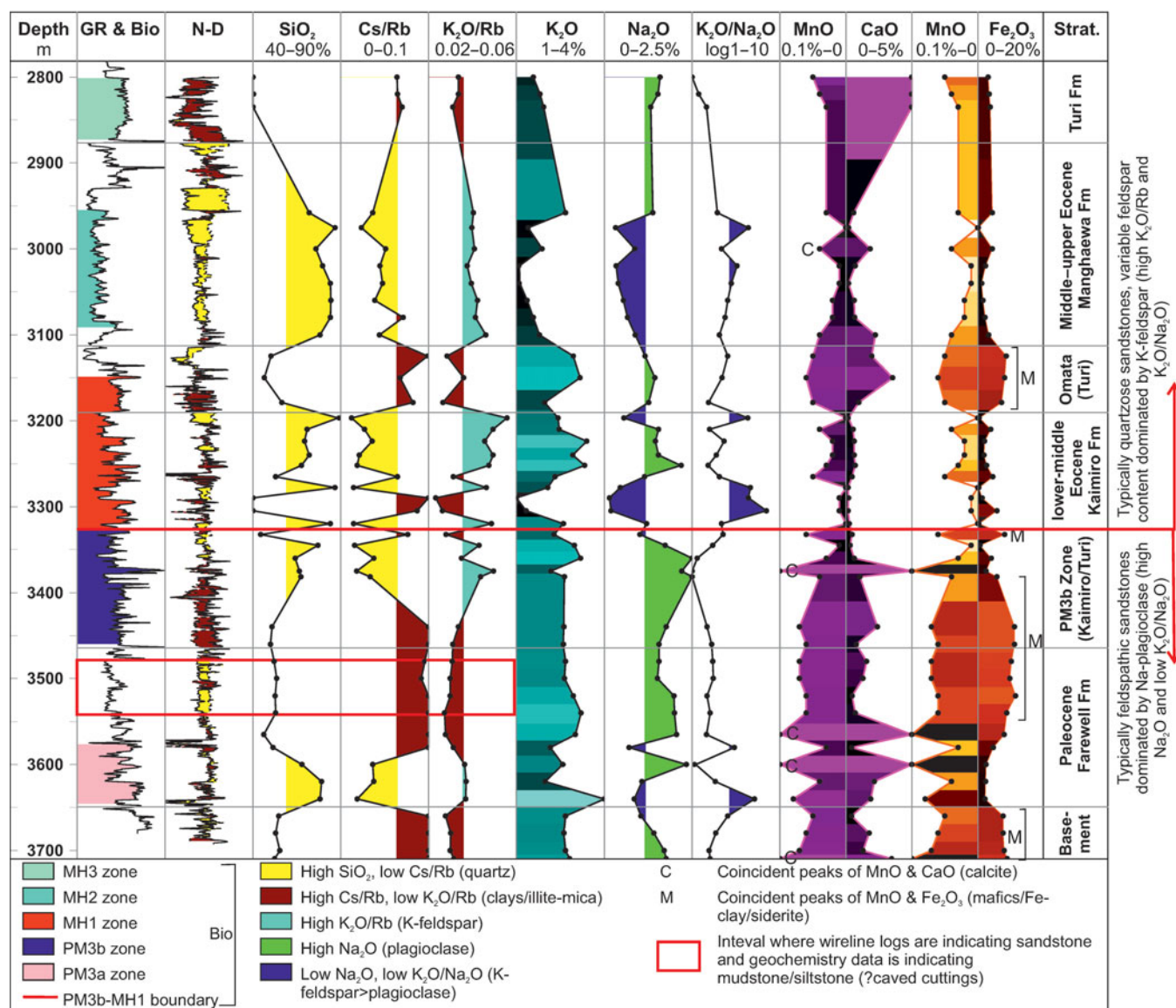
Fig. 7. (Colour online) Bulk-rock elemental data for key elements and ratios plotted against gamma-ray (GR), neutron-density (N-D) and biostratigraphy (Bio) data for well Maui B-P(8). Mudstone/siltstone intervals are indicated by high GR and brown shading on the N-D log crossover, while mudstone/siltstone cuttings are indicated by low SiO_2 and K_2O/Rb together with high Cs/Rb (shown by brown shading on Cs/Rb and K_2O/Rb profiles). Note that locally the geochemical data are not representative of the drilled interval (shown by red box and demonstrated by an elevated chem-GR in online Supplementary Material S2).

stratigraphic and/or geographic changes. Previous workers have used major oxide ratios of SiO_2, Al_2O_3 and, to lesser extents, MgO and Fe_2O_3 to distinguish sandstone lithologies from mudstone/siltstone (e.g. Sprague *et al.* 2009; Ikhane *et al.* 2014). However, it is clear that high Al_2O_3 concentrations in Palaeogene samples do not necessarily reflect mudstone/siltstone lithologies due to the presence of locally feldspathic and kaolinitic sandstones. In this study, an SiO_2/Al_2O_3 ratio of > 4 together with low Cs/Rb and high K_2O/Rb ratios (typically ≤ 0.05 and ≥ 0.035, respectively) have been used for sandstone identification.

4.d.1. MB-P(8)

Middle–upper Eocene sandstones (Mangahewa Formation, zone MH2) are typically characterized by high SiO_2 (72–87 wt%, mean 81 wt%), low K_2O (1.1–2.7 wt%, mean 1.6 wt%) and low Na_2O values (1.1–2.7 wt%, mean 0.7 wt%; Fig. 7). These results suggest

that the sandstones are quartzose with low volumes of total feldspar. Relatively high K_2O/Rb ratio values (> 0.037) indicate that much of the available K_2O is associated with K-feldspar rather than illite/mica, while relatively high K_2O/Na_2O ratio values (c. 2–4.5) indicate that within these feldspar-poor sandstones, K-feldspar is more abundant than Na-feldspar (albite). This interval is also characterized by very low background MnO and CaO, with a rare coincident peak interpreted to represent the local presence of minor carbonate cements (C in Fig. 7).

Lower–middle Eocene sandstones from MB-P(8) (Kaimiro Formation, zone MH1) also contain some samples with high SiO_2 (up to 89 wt%) with a similar major-element signature to the younger Mangahewa Formation. However, several samples from the Kaimiro Formation are characterized by lower SiO_2 (68–89 wt%, mean 77 wt%) associated with variable Na_2O (0.4–2.1 wt%, mean 1.3 wt%) and very high K_2O (2.1–3.4 wt%, mean

2.7 wt%), suggesting that locally the sandstones are relatively feld-spathic. Very high K_2O/Rb ratio values (up to *c.* 0.055) are again evidence that K_2O is mostly associated with K-feldspar (Fig. 7).

Sandstone samples of earliest Eocene (zone PM3b) and Paleocene (zone PM3a) age display a variable low-to-moderate SiO_2 content (64–77 wt%, mean 69 wt%). High SiO_2 contents (i.e. $SiO_2 > 80$ wt%) are not recorded through this interval, which is likely due to the relatively high K_2O (2.2–3.2 wt%, mean 2.7 wt%) and consistently high Na_2O (1.7–2.8 wt%, mean 2.4 wt%) below the MH1/PM3b zonal boundary (Fig. 7). High K_2O and Na_2O values are interpreted to reflect highly feldspathic sandstone compositions, while very low K_2O/Na_2O ratio values (1–1.7) indicate that Na-feldspar (albite) is likely to be more abundant than K-feldspar. This change in major-element concentration highlights a significant difference in sandstone composition between the older (Paleocene and earliest Eocene) and the younger (Eocene) sandstones.

The K_2O/Rb ratio appears slightly suppressed in the Paleocene sandstones (zone PM3a) compared with Eocene sandstones (zones PM3b to MH2), and this could be an indication of relatively high clay contents within the stratigraphically older deposits (Fig. 7). Sharp coincident peaks of MnO and CaO are again interpreted within the lowermost Eocene and Paleocene interval (zones PM3b and PM3a) to represent carbonate-cemented zones (C in Fig. 7). However, background MnO and CaO concentrations in Paleocene–lowermost Eocene lithologies are higher than those of overlying Eocene lithologies (zones MH1 and MH2), which could potentially reflect a change in clay, feldspar and/or cement mineralogy.

4.d.2. Regional correlation

Multi-well plots of key elemental data and ratios show that the significant change in Na_2O content, observed close to the PM3b/MH1 zonal boundary in well MB-P(8), also occurs in other study wells. Above the PM3b/MH1 boundary, most sandstone intervals are characterized by high SiO_2, high K_2O/Rb ratios and relatively low Na_2O values, suggesting that they are dominated by quartz and K-feldspar with relatively minor plagioclase. Below the PM3b/MH1 boundary, most sandstone intervals are characterized by lower SiO_2 and higher Na_2O, reflecting a plagioclase-rich affinity (Fig. 8).

Background MnO and CaO levels are low throughout much of the Eocene section (zones MH1 and MH2, Fig. 9), although local spikes of MnO (without coincident CaO spikes) do occur in some of the mudstone/siltstone intervals, and likely represent concentrations of Mn in clays and/or heavy minerals. Coincident peaks of MnO and CaO, interpreted to represent carbonate-cemented zones, are particularly prolific through the Eocene section at Kapuni-13 (Fig. 9). Overall, background MnO and CaO are higher in the older Paleocene and Cretaceous strata (zones PM3a and PM2), associated with the higher concentrations of Na_2O (Fig. 9) and with relatively high concentrations of TiO_2, Fe_2O_3, MgO, P_2O_5 and many trace elements (Table 3). It is suggested here that the higher CaO content reflects a component of Na–Ca plagioclase, which has been shown from QEMSCAN data (Higgs, 2010; Higgs *et al.* 2012b) to be very rare in Eocene strata of the Taranaki Basin but relatively common in Paleocene and Cretaceous strata. It is notable that the presence of Na–Ca plagioclase is associated with high total feldspar and where plagioclase is more abundant than K-feldspar (Fig. 10). Elevated levels of other elements in the older strata are interpreted to reflect an increase in the abundance of mafic and/or heavy minerals (e.g. TiO_2, MnO, Nb, Sc, Y, REEs) and a change in phyllosilicate

mineralogy to higher biotite and possibly chlorite/smectite (e.g. Fe_2O_3, MgO, REEs).

These geochemical results are evidence for a regional change in sandstone composition across the PM3b/MH1 zonal boundary. However, the trend is complicated by the fact that the lowermost Eocene deposits (zone PM3b) are relatively argillaceous in many wells and represent a period of overall transgression across western Taranaki Basin. Another complication is that few Eocene strata are preserved at Kupe South-4, where only the lowermost part of the PM3b zone is present and the geochemical change in composition occurs at a slightly lower stratigraphic level (Figs 6, 9). The change in composition is abrupt in most wells, with the exception of Turangi-3, which is the most distal study well and where a more gradual decline in Na_2O is observed from the PM3b zone upwards through the MH1 zone (Fig. 8).

A second, later regional change in major-element composition is suggested by a relatively gradual increase in Na_2O concentration, which has been observed towards the top of the study interval (Fig. 8). This increase in Na_2O in uppermost Eocene deposits (zone MH3) may reflect a return to relatively plagioclase-rich deposits and/or an upwards increase in smectite content. The increase in Na_2O is accompanied by an increase in CaO, which could either be related to the reintroduction of Ca-plagioclase or could reflect a change towards carbonate-rich facies close to the Eocene–Oligocene boundary.

4.e. Alteration indices

Geochemical indices of alteration are high through all mudstone/siltstone-dominated intervals, which is primarily a response to high Al_2O_3 concentrations in these lithologies (Fig. 11). While alteration indices are variable through the sandstone lithologies, they are also locally very high (CIW, 75–90). Several authors have used these indices to describe the degree of mineral alteration (e.g. Parker, 1970; Vogel, 1975; Nesbitt & Young, 1982; Harnois, 1988; Fedo *et al.* 1995; Buggle *et al.* 2011), and it is possible that some very high indices in the Palaeogene sandstones could be indicative of significant chemical weathering. There are, however, inherent problems that need to be considered when interpreting alteration indices for stratigraphic studies (e.g. Garzanti & Resentini, 2016), and results should be evaluated in conjunction with other data.

Multi-well plots show that the highest sandstone alteration indices occur above the PM3b/MH1 boundary in wells Maui-4, MB-P(8) and Kapuni-13, decreasing slightly uphole in upper Eocene strata (MH2 and MH3 zones; Fig. 11). Very high indices are also apparent within slightly older deposits (uppermost zone PM3a–PM3b) below the top Eocene unconformity at Kupe South-4, associated with depleted Na_2O and CaO (Figs 6, 11). The lowest sandstone alteration indices occur in upper Cretaceous, Paleocene and lowermost Eocene strata at Maui-4, MB-P(8) and Kapuni-13 (zones PM2, PM3a and PM3b respectively). However, alteration indices are also relatively low through the Eocene section in the more distal wells Turangi-3 and Kowhai A-1R, with a further decline into the uppermost Eocene (Fig. 11). Differences between the Paleocene and Eocene cannot be determined in these two distal wells due to the dominance of fine-grained (clay-rich) lithologies through the penetrated Paleocene strata.

These results further support a significant change in sandstone composition resulting in an overall reduction in alkali elements relative to Al_2O_3 above the PM3b/MH1 boundary. This could have been caused by loss of plagioclase through weathering/diagenesis,
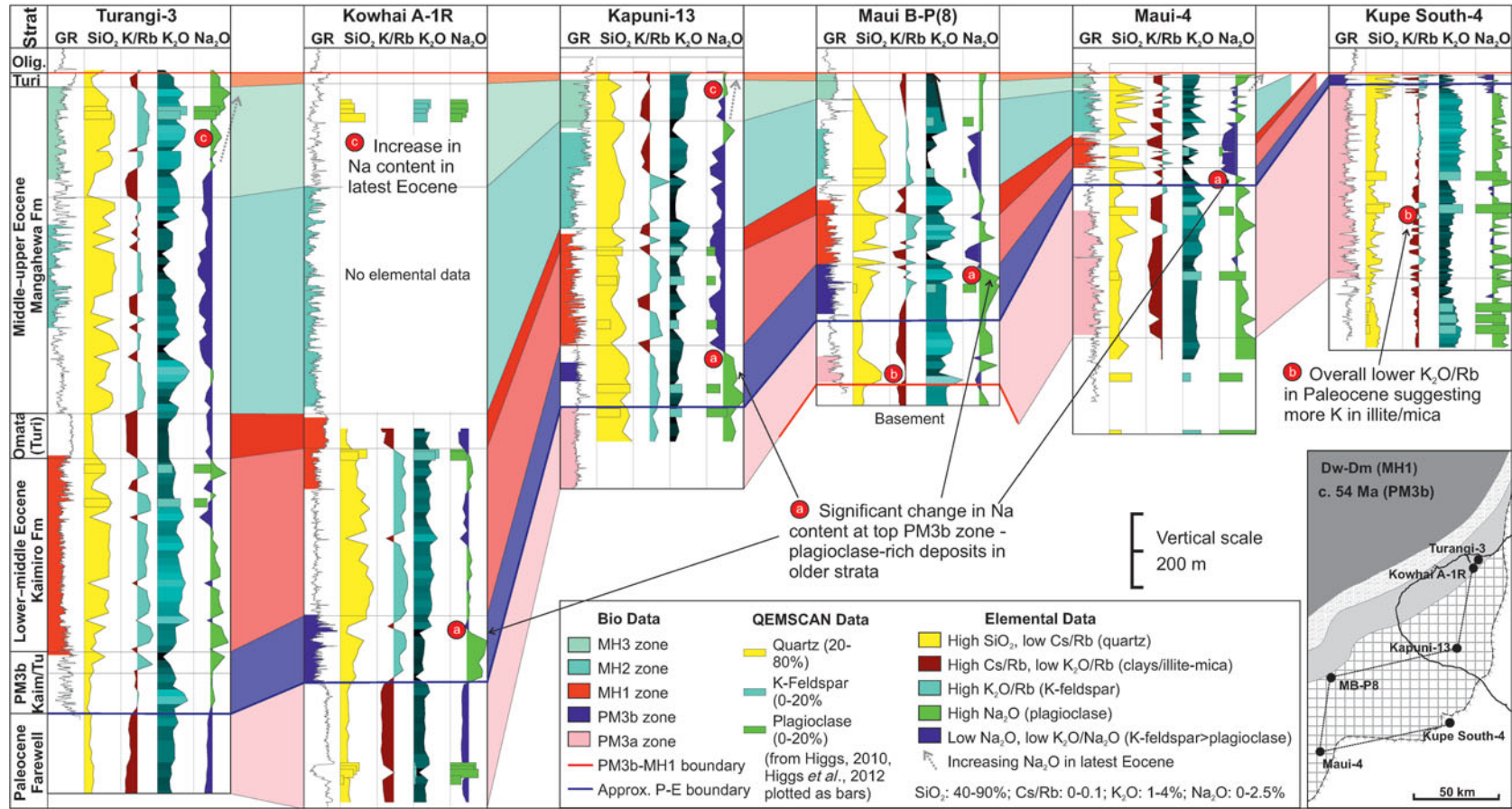
Fig. 8. (Colour online) Cross-section through study wells showing vertical changes in SiO$_2$, K$_2$O/Rb, K$_2$O and Na$_2$O plotted against gamma-ray (GR), biostratigraphy (Bio) and QEMSCAN data. Mudstone/siltstone cuttings are indicated by brown shading on K$_2$O/Rb data.
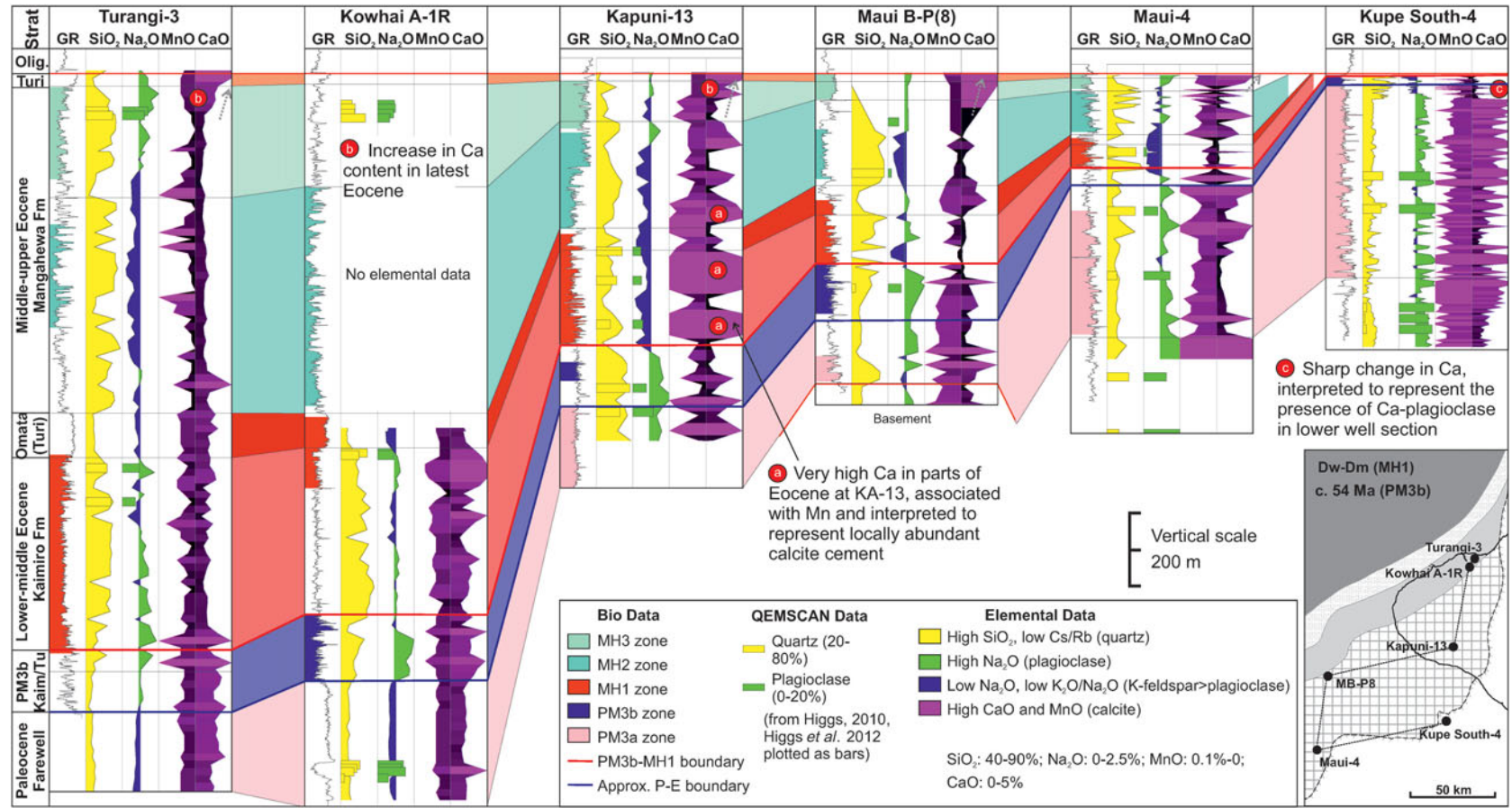
Fig. 9. (Colour online) Cross-section through study wells showing vertical changes in SiO_2, Na_2O, MnO and CaO plotted against gamma-ray (GR), biostratigraphy (Bio) and QEMSCAN data.

Table 3. Average abundance of selected oxides and trace elements by stratigraphy. All – all analysed cuttings; sand – sandstone cuttings based on lithology indicator cut-offs defined in Table 2. Eocene strata (representing MH1, MH2, MH3 zones) contain the lowest abundances of most elements, with the exception of Hf and Zr (zircon affinity), Cr and Ta.

	Na_2O (wt%)		MnO (wt%)		CaO (wt%)		TiO_2 (wt%)		Fe_2O_3 (wt%)		MgO (wt%)		P_2O_5 (wt%)	
	All	Sand	All	Sand	All	Sand	All	Sand	All	Sand	All	Sand	All	Sand
Eocene (MH1–3)	1.021	1.113	0.045	0.042	2.765	2.524	0.584	0.393	3.401	2.001	0.894	0.590	0.055	0.032
PM3b	1.459	1.697	0.057	0.052	2.452	2.862	0.671	0.492	4.467	2.663	1.110	0.797	0.057	0.040
Paleocene	1.489	1.839	0.075	0.111	3.578	5.068	0.796	0.472	5.373	2.914	1.576	0.799	0.097	0.083
Cretaceous	1.990	2.821	0.118	0.206	4.347	9.548	0.789	0.514	6.090	3.093	1.850	1.042	0.135	0.101

	Hf (ppm)		Zr (ppm)		Cr (ppm)		Th (ppm)		U (ppm)		Ta (ppm)		Cs (ppm)		Ga (ppm)	
	All	Sand	All	Sand	All	Sand	All	Sand	All	Sand	All	Sand	All	Sand	All	Sand
Eocene (MH1–3)	3.2	4.0	122.6	147.5	64.2	78.2	5.2	3.2	1.6	0.9	0.5	0.4	1.1	2.8	8.1	12.4
PM3b	3.7	4.4	138.5	163.4	75.0	85.6	6.1	4.3	1.6	1.0	0.5	0.4	1.2	3.2	10.2	14.1
Paleocene	3.1	4.3	116.3	155.8	44.5	69.0	7.9	3.8	2.2	1.0	0.5	0.3	1.8	5.6	11.2	17.5
Cretaceous	3.9	4.3	144.7	156.3	25.0	76.3	7.1	5.5	1.8	1.3	0.4	0.6	1.9	4.4	12.2	16.8
Common affinities	Zircon		Zircon		Heavy minerals		Zircon, apatite, monazite		Zircon, apatite, monazite		Ti-bearing heavy minerals		Clays		Clays	

	Nb (ppm)		Rb (ppm)		Sc (ppm)		Y (ppm)		Total REE (ppm)		La (ppm)		Yb (ppm)	
	All	Sand	All	Sand	All	Sand	All	Sand	All	Sand	All	Sand	All	Sand
Eocene (MH1–3)	4.2	5.5	49.4	58.2	5.0	9.0	7.1	12.5	45.0	69.6	13.3	9.0	1.3	0.7
PM3b	4.1	5.3	41.9	54.5	7.5	11.3	8.9	13.6	64.9	84.9	16.4	13.1	1.5	0.9
Paleocene	3.7	6.1	49.5	69.7	8.2	15.1	12.8	19.7	70.3	103.1	18.7	13.5	2.0	1.2
Cretaceous	6.2	5.7	60.3	65.4	7.7	15.2	15.7	20.3	94.2	103.7	18.7	20.1	2.0	1.4
Common affinities	Anatase, rutile, sphene, opaques		Mica		Clays, mafic volcanics, clinopyroxene		Zircon, garnet		Clays, mica, heavy minerals		Clays, apatite, monazite		Clays, garnet, zircon, xenotime	
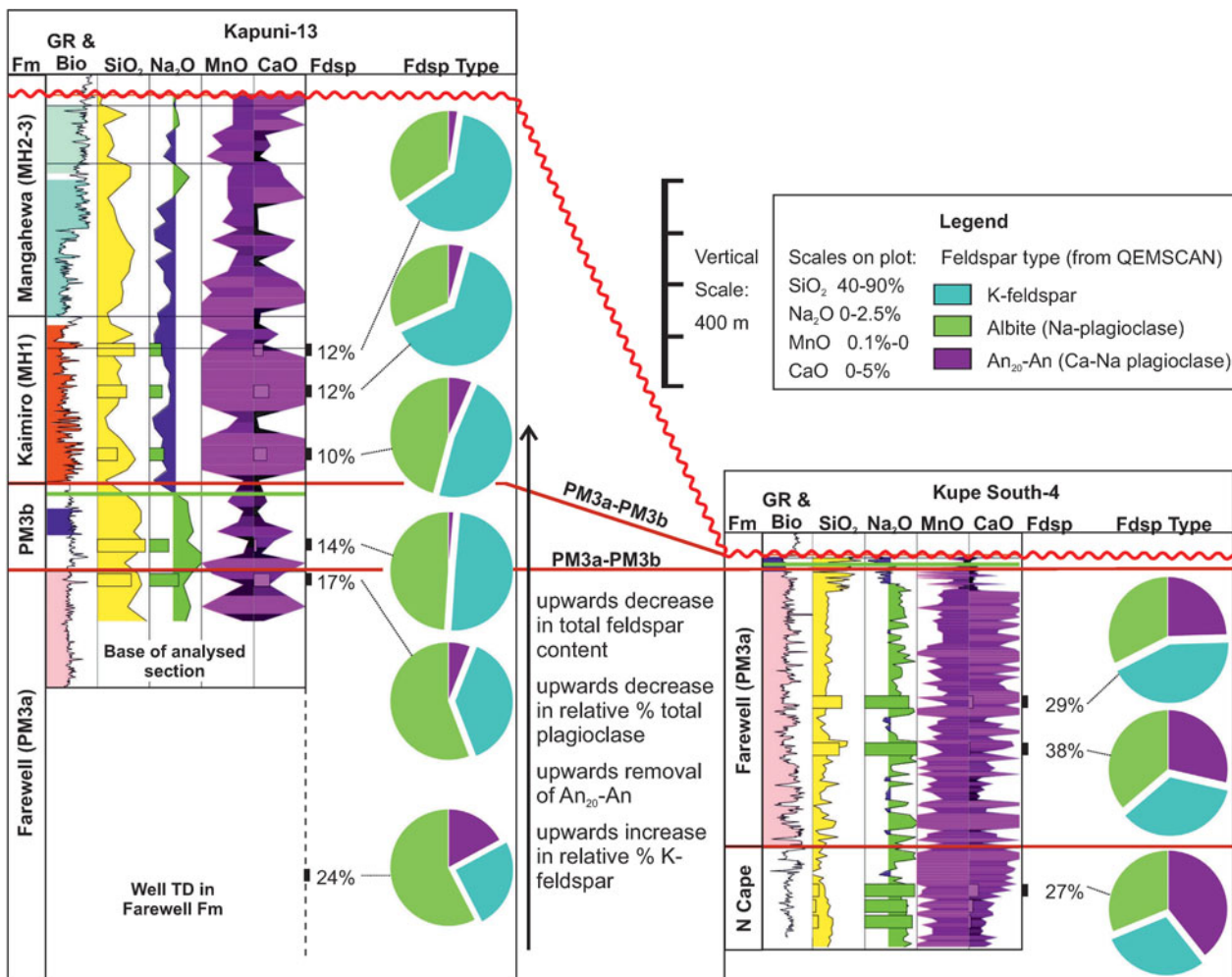
Fig. 10. (Colour online) Relative proportions of feldspars from QEMSCAN data (Higgs *et al.* 2012*b*) with bulk-rock elemental data (this study) plotted against gamma-ray (GR) and biostratigraphy (Bio) data for wells Kapuni-13 and Kupe South-4. Fdsp refers to total feldspar abundance (vol%) to nearest percent; relative proportion of feldspar types are illustrated by pie charts.

a change in sediment provenance and protolith composition, and/ or due to sedimentary/hydrodynamic effects.

4.f. Heavy mineral analysis, Kupe South-4 and -6

The main components of heavy mineral assemblages at Kupe South-4 and -6 are tourmaline, titanite (sphene), zircon and apatite (Table 4), all of which are common accessory minerals in granitoid rocks. Less abundant are epidote and garnet, both of which are commonly associated with greenschist-facies metamorphic rocks, but are also indicative of some intrusive rocks. Although variations are observed between the samples, overall the heavy mineral suites of Kupe South-4 and -6 are comparable to suite 4 of Smale (1992), which has previously been interpreted to represent derivation from metamorphic and granitic rocks of the NW Nelson area.

Results show high recovery of heavy minerals for three samples from Kupe South-4 and three samples from Kupe South-6; all are from the Paleocene (zone PM3a). A significant reduction is observed in the two samples taken near the P/E boundary with very few heavy minerals recovered from the single lower Eocene sample (zone PM3b). This uphole reduction in heavy mineral abundance is accompanied in Kupe South-4 by a significant increase in the proportion of ultrastable tourmaline, which is particularly

abundant in the lower Eocene sample. Both wells are characterized by an uphole increase in the ZTR (zircon–tourmaline–rutile) index (Table 4), and all heavy minerals, with the exception of zircon, show significant corrosion features. Collectively, these data might imply that the uppermost (younger) samples have a heavy mineral signature indicative of greater degrees of chemical/mechanical weathering compared with the lower samples.

Samples with the lowest amounts of both tourmaline and zircon (Kupe South-4, 3116.9 and 3321 m, Kupe South-6, 3300 m) are dominated by titanite (sphene), which can largely account for the high TiO$_2$ recorded in Paleocene strata and Eocene mudstones. These samples also contain the highest proportion of epidote (8.2–17.9 vol% of heavy mineral fraction), which is less stable than zircon and tourmaline. It is notable that small amounts of olivine and orthopyroxene have been identified from the sample taken from the top of the Paleocene strata in Kupe South-4 (3082.7 m); orthopyroxene has only been identified in very small quantities in two other samples. Both olivine and orthopyroxene are particularly unstable; their initial abundances (i.e. at the time of sediment deposition) might therefore have been higher, representing remnants of a largely altered heavy mineral suite derived from ultramafic–mafic igneous rocks. Alternatively, the very low abundance of these minerals might be indicative of an additional
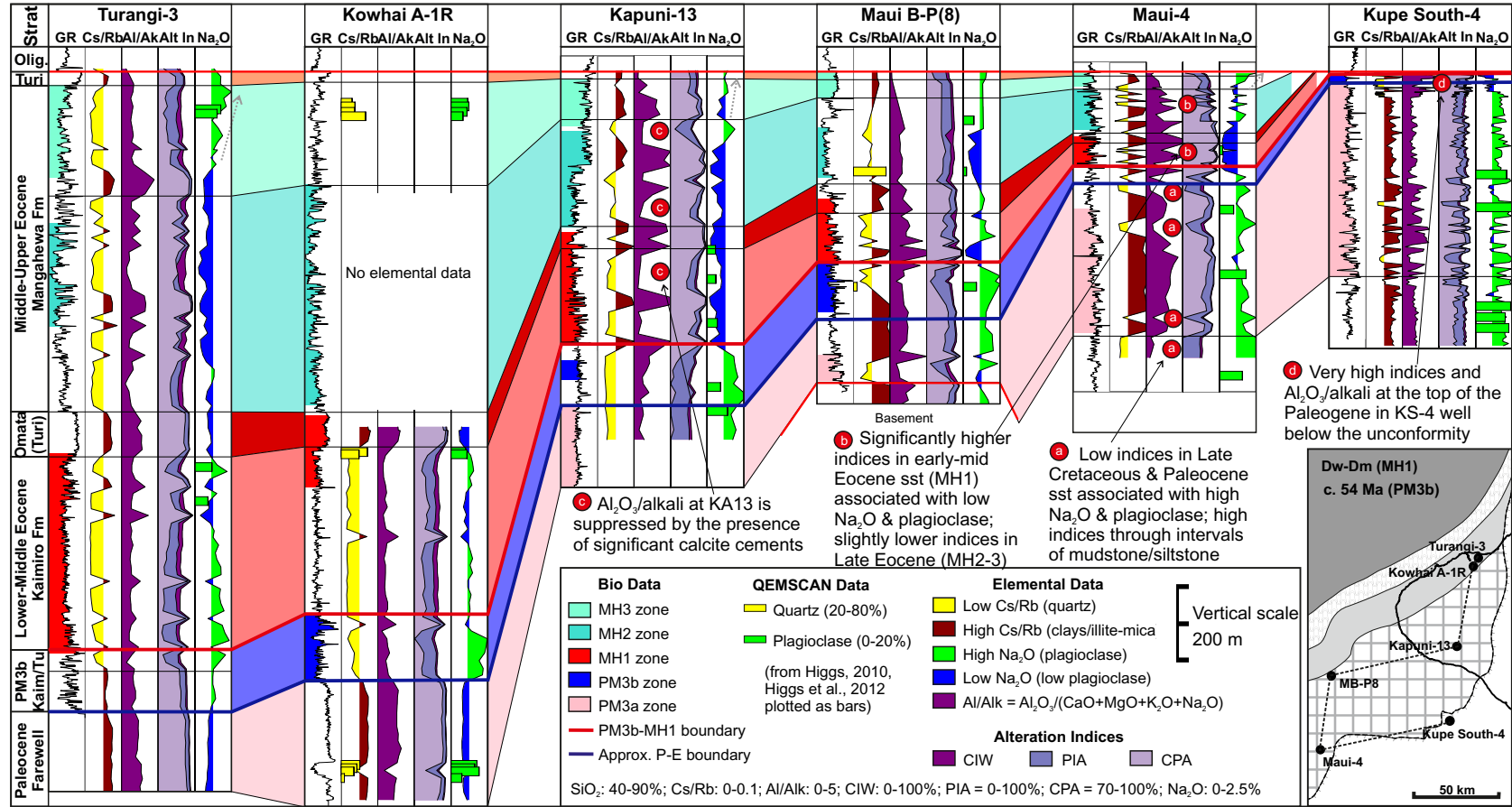
Fig. 11. (Colour online) Cross-section through study wells showing vertical changes in Cs/Rb, Al_2O_3/Alkali (Al/Ak = Al_2O_3/($CaO+MgO+K_2O+Na_2O$)), alteration indices (Alt In) and Na_2O plotted against gamma-ray (GR) and biostratigraphy data (Bio). Molecular proportions have been used in the calculation of alteration indices, where CaO* is the estimated silicate Ca. CIW – chemical index of weathering ((Al_2O_3/($Al_2O_3+CaO*+Na_2O$))×100; Harnois, 1988); PIA – plagioclase index of alteration ((($Al_2O_3-K_2O$)/($Al_2O_3+CaO*+Na_2O-K_2O$))×100; Fedo *et al.* 1995); and CPA – chemical proxy of alteration ((Al_2O_3/($Al_2O_3+Na_2O$))×100; Buggle *et al.* 2011). Mudstone/siltstone cuttings are indicated by brown shading on Cs/Rb data.

Table 4. Heavy mineral abundance (vol%) from wells Kupe South-4 and Kupe South-6. Other – sum of abundance of amphibole, anatase, andalusite, clinozoisite, clinopyroxene, diaspore, sillimanite and topaz; co – core; cu – cuttings

Depth (m)	Apatite	Cr-spinel	Epidote	Garnet	Olivine	Orthopyrox	Rutile	Titanite sphene	Tourmaline	Zircon	Other	Total grains	ZTR
Kupe South-4													
3057 (co, PM3b)	21.4	0	7.1	7.1	0	0	0	7.1	42.9	14.3	0	14	57.2
3082.7 (co, PM3a top)	32.4	0	2.7	10.8	5.4	2.7	0	13.5	18.9	13.5	0	37	32.4
3116.9 (co, PM3a)	0.7	0	17.9	4.5	0	0	3.7	61.2	3.7	6.7	1.5	134	14.1
3321 (cu, PM3a)	14.4	1.3	13.1	5.9	0	0	0	49.7	2.0	11.8	2.0	153	13.8
3588 (cu, PM3a base)	21.3	0	1.3	15.0	0	0	0	31.3	6.3	25.0	0	160	31.3
Kupe South-6													
3030 (co, PM3a)	10.8	5.4	5.4	18.9	0	0	0	10.8	5.4	45.9	2.7	37	51.3
3075 (cu, PM3a)	23.2	0	0	11.6	0	1.1	0	12.6	6.3	44.2	0	95	50.5
3203–3204.8 (co, PM3a)	14.3	1.9	1.9	14.3	0	0	0	22.9	7.6	35.2	1.0	105	42.8
3300 (cu, PM3a)	2.9	0	0	5.9	0	1.2	1.2	57.1	1.8	17.1	4.7	170	20.1

(minor) sedimentary source. Absence from the uppermost (late Eocene) sample could be due to complete dissolution within a highly altered zone, or a change in the sediment source.

4.g. Basement–sandstone correlation

The quartzo-feldspathic composition (Sections 4.c, 4.d) and heavy mineral suite (Section 4.f) of lower–middle Palaeogene sandstones in Taranaki Basin is consistent with a dominant source from the Tuhua Intrusives. Additionally, chondrite-normalized REE plots for the Palaeogene samples are comparable to REE profiles of the igneous basement samples from MB-P(8) and Maui-4, showing enrichment of LREE over HREE (see online Supplementary Material S5, available at http://journals.cambridge.org/geo). Very slight to moderate negative Eu anomalies are evident for most Palaeogene samples, which could suggest a dominant felsic source rock, but alternatively could be related to loss of plagioclase during weathering. Clear evidence for Na_2O depletion (and in some cases CaO depletion), reflecting a reduction in plagioclase content, has been noted in Eocene strata relative to the igneous basement samples and to Cretaceous–lowermost Eocene strata (Fig. 12).

High-field-strength elements associated with heavy minerals are unlikely to have been influenced by weathering or diagenesis, and are therefore commonly used in provenance studies (e.g. McLennan *et al.* 1993). Positive trends have been observed for several elements, although many relationships are fairly broad, suggesting that most elements are associated with a variety of heavy minerals. At least two positive trends, related to well location but unrelated to stratigraphy, are developed between some immobile elements. For example, samples of Cretaceous–Eocene age from Kupe South-4 and Kapuni-13 display lower Nb/TiO_2 and Ta/Nb, and higher TiO_2/Ta, Th/Ta and U/Ta compared with samples from other study wells (see online Supplementary Material S4). These plots confirm that there was a spatial change in sediment provenance across the study area, with the HFSEs interpreted to reflect contributions of heavy minerals derived from different igneous suites. Overall, trace-element ratios of Palaeogene sandstones from MB-P(8), Turangi-3 and Kowhai-A1R are most similar to published data from the Separation Point Suite, while Cretaceous and Palaeogene sandstones from Kapuni-13 and Kupe South-4 have more mafic compositions that are most similar

to data from the Darran Suite (e.g. Fig. 13a). There is no clear evidence for a dominant source from the Karamea Suite in any of the study wells (e.g. high Nb, Rb; Figs 4, 13a).

Detrital zircon age data are available from a previous study for a single Cretaceous sandstone within the sampling interval at Maui-4 (2841–2844 m; Adams *et al.* 2017), confirming provenance from the Tuhua Intrusives. However, zircon ages also show that there has been input from several different igneous suites (*c.* 44% zircon from the Separation Point/Rahu Suite, 13% from the Darran Suite, 29% from mid-Palaeozoic suites, 13% from Buller/Takaka metasedimentary rocks). Notably, while detrital zircon data suggest that Separation Point Suite was the dominant source for this Maui-4 sample, the Y–Nb plot indicates that the Darran Suite was dominant (Fig. 13a). This discrepancy could perhaps be explained by lower zircon fertility of the Darran Suite, although that would need to be proven from further research. It is suggested here that several igneous suites are likely to have contributed sediment to the Palaeogene interval at all study locations (cf. Higgs & King, 2018), which, together with the wide-ranging composition of suites, makes source identification from geochemistry problematic.

In addition to spatial trends in immobile trace elements, some trends have been observed that appear related to stratigraphy. Overall, the Cretaceous–Paleocene lithologies display a much tighter geochemical signature compared with a more variable geochemistry of Eocene lithologies, while the few samples from uppermost Eocene strata have compositions that are most similar to the Cretaceous–Paleocene samples (Fig. 13). Other observed trends are not consistent across all locations, and probably reflect local changes in source area with time (Fig. 13a). Notably, however, enrichment of Hf and Zr occurs relative to Sc within many Eocene sandstones from all wells (Fig. 13b). Given the strong affinity of Hf and Zr with zircon (see online Supplementary Material S4), this could either imply removal of relatively reactive minerals prior to deposition (i.e. enhanced chemical and/or physical weathering), or an uphole change to a more felsic, zircon-rich sedimentary source. The former is favoured here because La/Sc and Th/Sc remain approximately the same, while Zr/Sc and Hf/Sc increase sharply; Th/Sc and La/Sc would be expected to track Zr/Sc and Hf/Sc if the relative zircon enrichment was primarily due to a change in provenance. It is also notable that in most wells the Cr/Y ratio values increases in Eocene sandstones, being locally
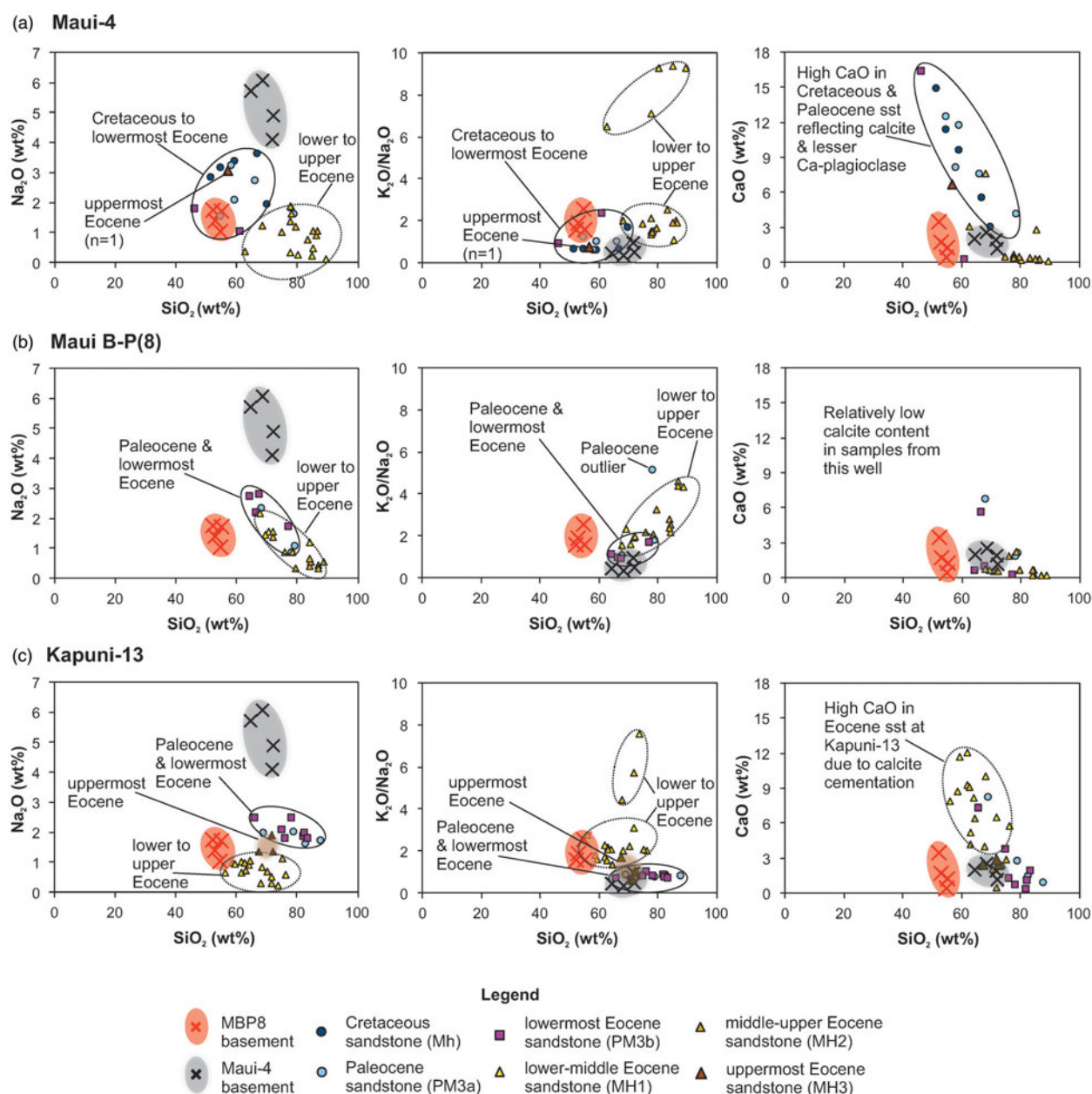
Fig. 12. (Colour online) Selected cross-plots showing the distinct major-element composition of basement samples at Maui-4 and Maui B-P(8) and a comparison between basement and Paleocene sandstone composition in wells (a) Maui-4, (b) Maui B-P(8) and (c) Kapuni-13, where sandstone lithology has been based on a cut-off for SiO_2/Al_2O_3 and K_2O/Rb. Plots illustrate the higher Na_2O content of Cretaceous to lowermost Eocene sandstones (PM3a, PM3b) and uppermost Eocene sandstones (MH3) compared with the main Eocene reservoir sandstones (MH1 and MH2).

higher than Cr/Y values from published data for the Tuhua Intrusives, and significantly greater than Cr/Y values of both Eastern and Western Province metasedimentary rocks (e.g. Roser *et al.* 2002). As Cr and Y are both relatively immobile elements, if they co-exist in a mineral then relative enrichment of Cr over Y due to chemical weathering/alteration is unlikely. However, high Cr/Y values could be explained if the Cr originated from resistant heavy minerals (e.g. tourmaline, rutile, titanite and ilmenite/magnetite) and Y was at least partially present (and lost) in relatively reactive heavy minerals (e.g. garnet). High Cr/Y ratios could also reflect concentrations of clinopyroxene (i.e. increased mafic material input); however, clinopyroxene is very unstable and high concentrations would be diametrically opposed to zircon

enrichment. On this basis, it is suggested that relatively high Cr within some of the Eocene sandstones is most likely due to concentrations of resistant heavy minerals, either resulting from an evolving sediment provenance (relatively enriched in these minerals) or from enhanced chemical/physical weathering.

Overall, the trace-element data from Kupe South-4 is very constant, suggesting that at this location there has not been an appreciable change in provenance through Cretaceous–earliest Eocene time. However, there is a very clear change in some HFSE occurring at the same stratigraphic level as a significant change in the major-element geochemistry (Fig. 6). Elevated Hf/Sc and Zr/Y show a good match with high Ta/HREE, Cr/Ce, Cr/Y and Cr/Th, which is interpreted to represent relative zircon and Cr-bearing
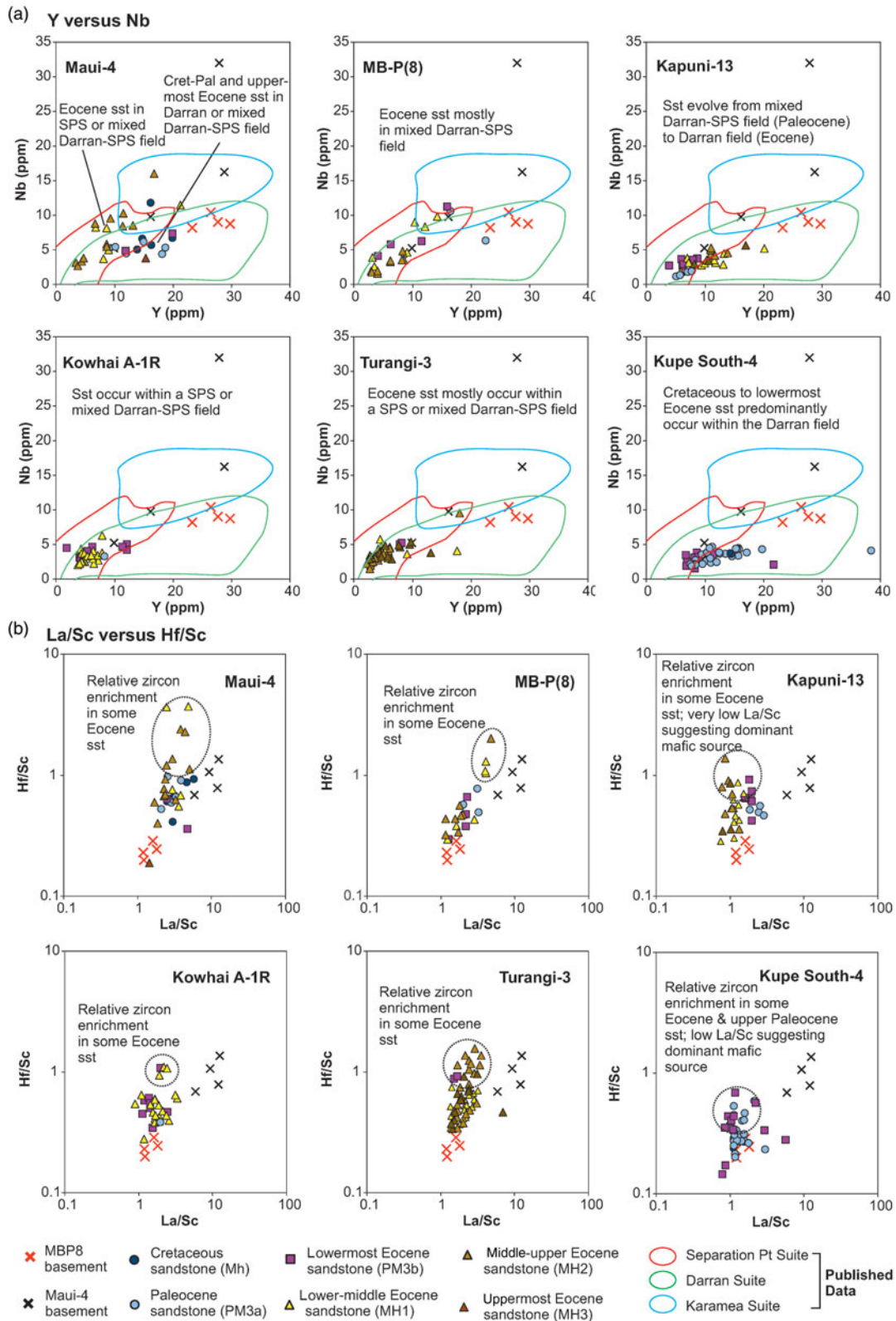
Fig. 13. (Colour online) Geochemical plots for basement and sandstone samples from all study wells showing (a) Y v. Nb; and (b) La/Sc v. Hf/Sc. Sandstone lithology has been based on a cut-off for SiO_2/Al_2O_3 and K_2O/Rb. (a) > 90% data fields based on published geochemical data from selected igneous suites (references provided in online Supplementary Material S3).
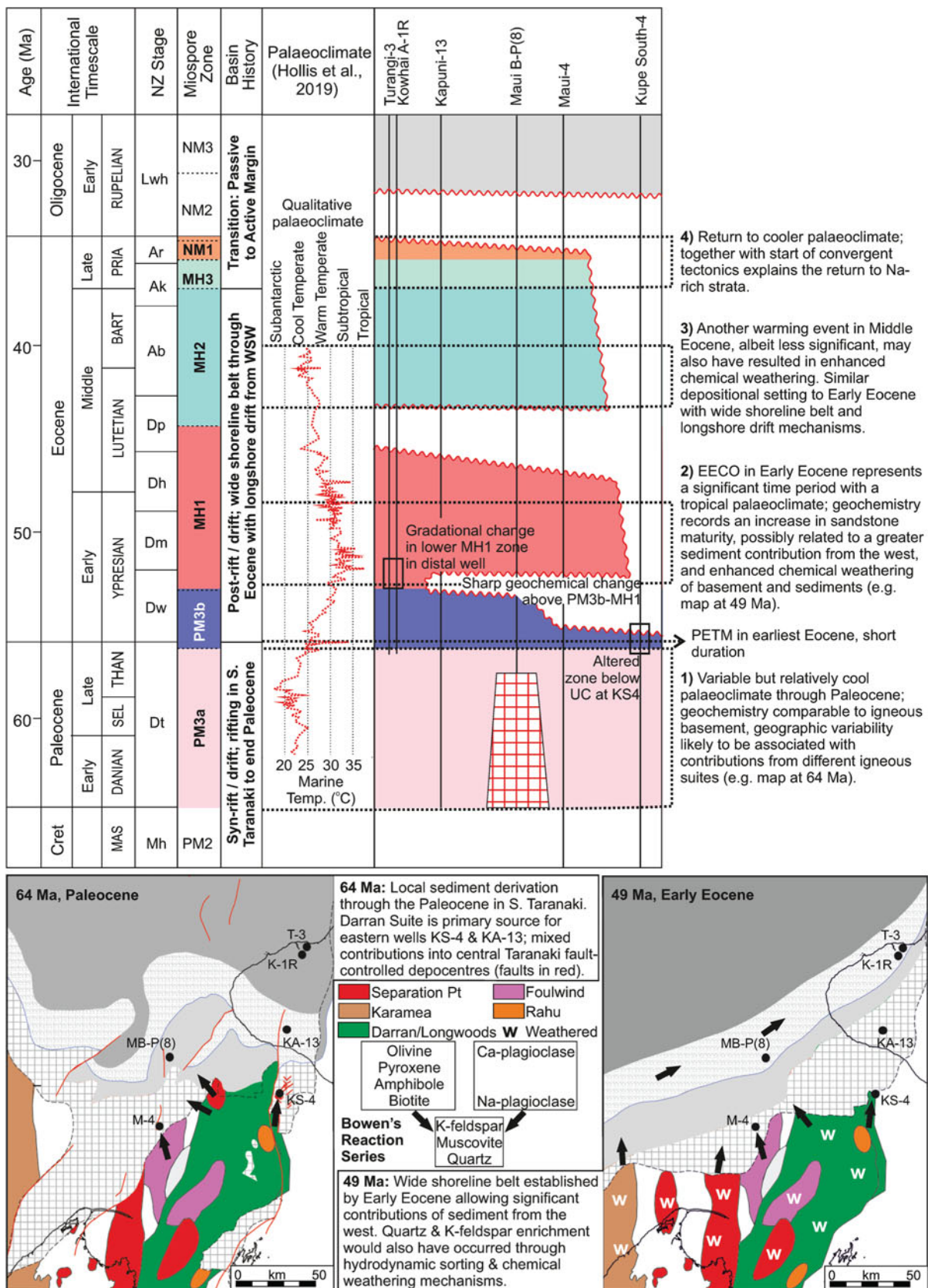
Fig. 14. (Colour online) Summary figure showing the interpretations for the observed stratigraphic changes in major-element geochemistry and quartz–feldspar composition. The stratigraphic framework is modified from King & Thrasher (1996), international timescale from Gradstein *et al.* (2012) and miospore zones from Raine (1984, 2004). The Taranaki basement map is modified from Tulloch & Mortimer (2017) and palaeogeography maps modified from Strogen (2011). The Palaeogene palaeoclimate estimate is based on TEX_{86}^{H} records for New Zealand (red dashed line being the 3-point moving average), which is a proxy for sea surface temperature, from Hollis *et al.* (2019).

heavy mineral enrichment, and is consistent with a change in the heavy mineral suite from sphene-dominated (Paleocene) to zircon-tourmaline (lowermost Eocene). Given the constant ratios of other immobile trace elements, together with high alteration indices and extensive kaolinitization (Martin *et al.* 1994) of uppermost Eocene strata, these data imply that the significant differences in major-element composition between the older and younger strata in this well is indeed primarily due to alteration.

5. Discussion

Clear trends in major-element geochemistry have been observed through the Cretaceous–Eocene succession in Taranaki Basin that relate to stratigraphic changes in sandstone composition. Paleocene (and Upper Cretaceous) sandstones display a mineralogy that is most comparable to the plutonic basement rocks that underlie much of the basin and crop out in the northern South Island (Tulloch, 1983, 1988; Mortimer *et al.* 1997; Rattenbury *et al.* 1998). These rocks are composed primarily of plagioclase (up to *c.* 50 vol%, mostly albite with locally significant An_{60}) with subordinate quartz, K-feldspar, biotite and minor clay and heavy minerals. By comparison, Eocene sandstones display a mineralogy that is enriched in quartz and K-feldspar compared with both Paleocene sandstones and known basement compositions. The most significant change in geochemical signature occurs across the PM3b/MH1 zonal boundary and is abrupt in relatively proximal wells Maui-4, MB-P(8) and Kapuni-13, but appears more gradual in the most distal well Turangi-3. We suggest that this could be due to fluvial incision, erosion and/or non-deposition in some of the relatively proximal wells in response to the Kaimiro sequence boundary (cf. Higgs *et al.* 2017) (Fig. 14). A more subtle change back to relatively sodic plagioclase-rich sandstones also occurs in uppermost Eocene strata (miospore zone MH3). Possible reasons for the observed stratigraphic changes in Palaeogene mineralogy are discussed below.

5.a. Change in sediment provenance

The earliest Eocene period (PM3b zone, Fig. 2) marks the onset of the post-rift phase in parts of southern Taranaki (King & Thrasher, 1996; Strogen *et al.* 2017), which resulted in flooding of Paleocene depocentres and deposition of marine mudstone across much of the southern basin. All the central basement ridges would have become submerged, and subsequent Eocene strata were deposited on an intra-continental passive margin that was virtually undisrupted by contemporaneous faulting (King & Thrasher, 1996; Stagpoole & Nicol, 2008; Strogen, 2011). It therefore seems plausible that a change in sedimentary provenance might have occurred in response to this significant change in the southern basin morphology during latest Paleocene–earliest Eocene time.

Despite changes in tectonic regime, the distribution of preserved Paleocene and Eocene strata in Taranaki Basin is similar, and implies a southern eroding hinterland dominated by igneous intrusives and subordinate Western Province metasediments (Fig. 14). A slightly larger area of the southern hinterland may have been exposed during Eocene time, while drowned basement ridges that defined Cretaceous syn-rift sub-basins may have been capable of shedding some sediment during deposition over the Paleocene Epoch. Although the Tuhua Intrusives in the southern hinterland collectively formed the dominant sediment source throughout Palaeogene–Eocene time, there will have been subtle changes in contribution from the different plutonic suites as the drainage

patterns changed through time. Sediment contribution from meta-sedimentary rocks (Eastern and Western provinces) is unproven but not considered to have been dominant through Cretaceous–Eocene time, as supported by the limited detrital zircon data (cf. Higgs & King, 2018), dominance of igneous lithics (e.g. Martin *et al.* 1994; Chemostrat Ltd, 2017; Higgs *et al.* 2013, 2017) and geochemical signatures.

It is difficult to confirm or demonstrate changes in igneous source based on the bulk-rock geochemistry. This is partly because of the very wide range of chemical compositions recorded in the literature for individual suites, but also because of sediment contribution from multiple suites. Using current knowledge on the distribution of intrusives from Tulloch & Mortimer (2017), based purely on proximity, the dominant igneous source rocks for lower–middle Palaeogene sandstones may have been the Darran and Longwood suites in the east (Kupe South-4, Kapuni-13) and Separation Point or Foulwind suites in the west (MB-P(8), Maui-4), with possible local contribution from other less extensive suites (e.g. Rahu, Tobin and Tarpaulin suites; Fig. 14). The immobile trace-element geochemistry supports a mixed sedimentary source, and is also consistent with different source contributions to eastern and western parts of the basin that are related to basement proximity (Fig. 13a).

It is possible that the regional stratigraphic change from plagioclase-rich to quartz–K-feldspar-dominated sandstones reflects an overall change in provenance from dominantly intermediate–mafic sources to relatively felsic sources in the earliest Eocene. Known felsic sources include the I-type Separation Point, I-/S-type Rahu, and S-type Karamea and Ridge suites (e.g. Muir *et al.* 1995; Tulloch *et al.* 2009; Tulloch & Palin, 2013), with extensive Separation Point and Karamea granitoids mapped to the south and west of all study wells (Tulloch, 1988; Tulloch *et al.* 2009; Tulloch & Mortimer, 2017). These felsic granitoids are likely to have formed a more significant eroding hinterland during Eocene rather than Paleocene time (Fig. 14 and figs 11–13 of Higgs & King, 2018) and could explain the greater variability in geochemical signature of Eocene compared with Paleocene lithologies. Provenance for Paleocene sandstones in southern Taranaki (i.e. Manaia/Pakawau sub-basins) is therefore likely to have been from relatively local basement highs due to the residual rift basin topography (e.g. Smithies *et al.* 2019), while the provenance for Eocene sandstones may reflect more mixing and, potentially, sources from further afield. Relatively quartzose-, K-feldspar-rich Eocene sediments would have been transported via longshore drift across a broad shelf, with further quartz and resistant heavy-mineral enrichments from transportational winnowing, reworking and progressive weathering of less-resistant minerals. The geochemical data are, however, not entirely consistent with a simple change from dominantly mafic–intermediate sediment sources (Cretaceous–earliest Eocene) to felsic-sourced sediment (early–late Eocene). Instead, the trends observed in HFSE ratios are interpreted to reflect local changes in depositional facies, provenance and drainage patterns which are overprinted by the more significant regional change in major-element geochemistry, and detrital composition across the PM3b/MH1 boundary.

Major-element, immobile trace-element and petrographic data are all consistent with a return to plagioclase-rich deposits during latest Eocene time. This period represents the start of an episode of tectonic uplift and erosion in the eastern part of the basin, as a far-field manifestation of the proto Australian–Pacific plate boundary propagating to the east (Strogen *et al.* 2014, 2019). A dominantly mafic provenance is likely from either the exposed Tuhua

Intrusives in the south and SE, or from eroding Cretaceous–Paleocene strata located to the east of the present-day Taranaki Basin margin. Locally, Eastern Province zircons have been recorded from the NE part of Taranaki Basin in uppermost Eocene strata (e.g. Kamp, 2012), which, together with the introduction of metasedimentary lithic clasts in this part of the basin, would be consistent with some sediment derivation from the east at this time (Higgs & King, 2018).

5.b. Chemical weathering and/or alteration

Substantial evidence has been presented to suggest there has been preferential weathering and/or alteration of sediment during Eocene time; significant Na and Ca depletion is observed above the PM3b/MH1 boundary; elevated Hf/Sc, Zr/Y, Cr/Ce, Cr/Y and Cr/Th occur in Eocene deposits (indicating relative enrichment of zircon- and Cr-bearing heavy minerals); Eocene sandstones are impoverished in heavy minerals and dominated by a resistant suite compared with Paleocene sandstones; Eocene strata are characterized by higher alteration indices than older Cretaceous–Paleocene sandstones. These data are supported by other studies that have demonstrated considerable feldspar alteration within some Eocene sandstones associated with secondary kaolinite precipitation (e.g. Clews & Soo, 1994; Higgs *et al.* 2013, 2017), extensive kaolinite in the uppermost Paleocene–lowermost Eocene interval in the Kupe South Field reflecting alteration of unstable minerals (Martin *et al.* 1994), and extreme weathering observed at the top of the Paleocene outcrop (Smithies *et al.* 2019). This would all be consistent with enhanced mineral alteration in the lower Eocene strata of Taranaki Basin. It is also suggested that zones of carbonate cement, represented by elevated MnO and CaO in Eocene sandstones, might relate to alteration of original Ca–Na plagioclase; this feldspar composition is likely to have been more common in eastern wells that had a relatively mafic provenance, and would be consistent with redistribution of Ca into pervasive cements at Kapuni-13 (Fig. 10).

The effects of enhanced chemical weathering are usually observed in warm, humid (tropical) environments (cf. Nesbitt & Young, 1982), which may have occurred during the Paleocene–Eocene period associated with global warming events, such as the Paleocene–Eocene Thermal Maximum (PETM) and Early Eocene Climatic Optimum (EECO). The PETM, at *c.* 56 Ma, was a transient period of rapid global warming (by 4–8 °C, depending on depositional setting), associated with a massive input of ^{13}C-depleted carbon into the ocean–atmosphere system (e.g. Zachos *et al.* 2008; Murphy *et al.* 2010; McInerney & Wing, 2011). The EECO, extending from *c.* 53.3 to 49.1 Ma (Westerhold *et al.* 2018), represents the warmest sustained temperatures of the Palaeogene period, with atmospheric pCO_2 levels possibly exceeding 1000 ppm (Hollis *et al.* 2019). Data suggest that SW Pacific sea surface temperatures (SSTs) increased by more than 10 °C from late Paleocene to early Eocene time (Hollis *et al.* 2009, 2012; Bijl *et al.* 2013). Recent studies of the New Zealand region (Hollis *et al.* 2009; Crouch *et al.* 2020) also show that the long-term EECO warming started close to the PM3b/MH1 boundary, with the Mangaorapan Stage (zone MH1, early Eocene) characterized by a subtropical to tropical palaeoclimate (Fig. 14). It therefore seems likely that the longer-term EECO could have significantly increased the effect of chemical weathering in the Eocene strata compared with the underlying Paleocene deposits.

Enhanced chemical weathering in response to this warm early Eocene palaeoclimate will have modified exposed basement rocks

and sediments. Additionally, compared with short transport distances during Paleocene time, the broad Eocene coastal fairway will have subjected sediments to longer transport distances and greater reworking, thus exposing the sediment to the effects of chemical weathering for a longer time. Enhanced chemical weathering would have persisted into shallow burial (eodiagenesis), which is likely to have been most effective during periods of slow deposition in terrestrial or coastal regions or where the sediment was exposed to prolonged periods of exposure, possibly related to sequence boundaries. All of these processes could explain relative enrichment of stable detrital minerals (quartz- and K-feldspar) and authigenic kaolinite (an end-member for alteration/weathering processes; e.g. Nesbitt & Young, 1982; Fernández-Caliani *et al.* 2010; Buggle *et al.* 2011; Babechuk *et al.* 2014) in lower–middle Eocene strata, associated with the depletion of relatively unstable plagioclase and heavy minerals (cf. Bowen's reaction series, Fig. 14). A change back to slightly more Na_2O-rich (plagioclase-rich) compositions in uppermost Eocene strata could potentially be a response to gradual cooling after the Eocene warming events, associated with a reduction in the effects of chemical weathering. However, this is also the time when minor, southward-propagating uplift of the eastern basin margin was initiated, and a change in sediment provenance is considered likely (Higgs & King, 2018).

Quartz enrichment can also occur through diagenetic processes that are not related to chemical weathering and palaeoclimate. Previous workers have shown that Palaeogene sandstones in Taranaki have undergone significant alteration during burial diagenesis (e.g. Hill & Collen, 1978; Martin *et al.* 1994; Smale *et al.* 1999; Higgs *et al.* 2007, 2013) that has changed their mineralogical composition. In particular, the variable alteration of feldspar is reported, whereby feldspar reacts with acidic pore fluids to form secondary kaolinite, quartz and locally carbonate cement (Higgs *et al.* 2013, 2017). Since plagioclase feldspar is more reactive than K-feldspar, these reactions ultimately result in relatively quartz–K-feldspar-rich compositions compared with the original highly feldspathic sandstones. However, while these reactions appear to have been locally significant, they would not have resulted in the regional stratigraphically defined change in composition as observed at the PM3b/MH1 zonal boundary.

In summary, it is suggested that the stratigraphic changes observed in geochemical signature are, at least in part, related to the effects of variable weathering and alteration associated with changes in palaeoclimate and depositional environment during Palaeogene time. However, while a very clear alteration zone is observed at Kupe South-4 (Fig. 6), this is slightly older than the regional compositional change at the PM3b/MH1 boundary. At this location, the Eocene deposits are largely eroded (or non-deposited) and the alteration zone occurs just below a major angular unconformity with overlying Oligocene strata (cf. fig. 5 of Strogen *et al.* 2014); a detailed investigation of mineral paragenesis in the Kupe South Field forms part of another ongoing study.

6. Conclusions

Late Cretaceous–Paleocene sandstone lithologies have been defined on the basis of their bulk-rock geochemistry by a SiO_2/Al_2O_3 ratio of > 4 and K_2O/Rb ratio of > 0.035. The relative abundance of SiO_2, K_2O and Na_2O in the sandstones provides a good indicator of the relative abundance of quartz, K-feldspar and Na-

plagioclase. Trends in the concentration of Fe_2O_3, MgO, CaO and MnO are linked to the distribution of siderite–dolomite cements and reactive minerals, such as biotite, unstable heavy minerals, chlorite and Na–Ca plagioclase. Elevated Al_2O_3 is associated with a high clay content, mostly kaolinite.

A regional change in bulk-rock geochemistry is marked by a significant change in Na_2O, and occurs at the lowermost Eocene PM3b/MH1 zonal boundary, correlated to *c.* 53.5 Ma. Most Eocene sandstones are characterized by relatively high SiO_2, K_2O/Na_2O and K_2O/Rb values, and relatively low Na_2O, Al_2O_3, MgO, Fe_2O_3, MnO, CaO, TiO_2, Nb, Th, Cs, Ga, Rb, Sc, Y and REE values. Conversely, most Cretaceous and Paleocene sandstones are characterized by lower SiO_2, K_2O/Na_2O and K_2O/Rb values and relatively high Na_2O, Al_2O_3, CaO, MgO, Fe_2O_3, MnO, TiO_2, Nb, Th, Cs, Ga, Rb, Sc, Y and REE values.

Petrographic data show that the difference in chemical signature is largely due to a change from plagioclase-rich sandstones in Upper Cretaceous–Paleocene strata to quartz–K-feldspar sandstones in Eocene strata. This could partially reflect a change in provenance due to the evolving basin topography and palaeoenvironment. Cretaceous and Paleocene sandstones reflect local sources dominated by relatively plagioclase-rich granitoids of the Separation Point and Darran suites, and short sediment transport distances in rifted sub-basins. Conversely, Eocene sandstones are interpreted to represent a greater mixing of igneous sources with significant reworking by transportation winnowing and reworking. Immobile trace-element data and element ratios are consistent with a mixing of multiple igneous sources, and also demonstrate some spatial control on sediment provenance. However, there is substantial evidence for advanced feldspar alteration and relative enrichment of ultrastable heavy minerals in Eocene sandstones compared with Paleocene sandstones. A change in the bulk-rock geochemistry of lowest Eocene strata is therefore also likely to reflect enhanced chemical weathering of unstable grains, driven by significant long-term global warming (EECO).

Supplementary material. To view supplementary material for this article, please visit https://doi.org/10.1017/S0016756819001596

References

Adams CJ, Campbell HJ, Mortimer N and Griffin WJ (2017) Perspectives on Cretaceous Gondwana break-up from detrital zircon provenance of southern Zealandia sandstones. *Geological Magazine* **154**, 661–82.

Allibone AH, Jongens R, Scott JM, Tulloch AJ, Turnbull IM, Cooper AF, Powell NG, Ladley EB, King RP and Rattenbury MS (2009) Plutonic rocks of the Median Batholith in eastern and central Fiordland, New Zealand: field relations, geochemistry, correlation, and nomenclature. *New Zealand Journal of Geology and Geophysics* **52**, 101–48.

Babechuk MG, Widdowson M and Kamber BS (2014) Quantifying chemical weathering intensity and trace element release from two contrasting basalt profiles, Deccan Traps, India. *Chemical Geology* **363**, 56–75.

Bal AA (1994) Cessation of Tasman Sea spreading recorded as a sequence boundary: interpretation of an early Paleocene unconformity in the Pakawau sub-basin, northwest Nelson, New Zealand. In *The Evolution of the Tasman Sea Basin* (eds GJ van der Lingen, KM Swanson and RJ Muir), pp. 105–17. Proceedings of the Tasman Sea Conference, 27–30 November 1992. Christchurch, New Zealand: Balkema, Rotterdam.

Bartram KM, Sykes R and Crouch EM (1996) A correlation study of three wells in Kapuni Field, Taranaki Basin, New Zealand, using palynology and coal sulphur contents. Client Report 53552A, Institute of Geological & Nuclear Sciences, New Zealand, 51 p.

Bernet M and Bassett K (2016) Quartz types of the Eocene Broken River Formation, Mount Somers, South Island, New Zealand. *New Zealand Journal of Geology and Geophysics* **59**, 274–85.

Bijl PK, Sluijs A and Brinkhuis H (2013) A magneto- and chemostratigraphically calibrated dinoflagellate cyst zonation of the early Paleogene South Pacific Ocean. *Earth-Science Reviews* **124**, 1–31.

Bloch S (1994) Effect of detrital mineral composition on reservoir quality. In *Reservoir Quality Assessment and Prediction in Clastic Rocks* (ed MD Wilson), pp. 61–182. Society for Sedimentary Geology, Tulsa, SEPM Short Course 30.

Bradshaw JD (1989) Cretaceous geotectonic patterns in the New Zealand region. *Tectonics* **8**, 803–20.

Buggle B, Glaser B, Hambach U, Gerasimenko N and Marković S (2011) An evaluation of geochemical weathering indices in loess-paleosol studies. *Quaternary International* **240**, 12–21.

Bull S, Nicol A, Strogen D, Kroeger KF and Seebeck HS (2019) Tectonic controls on Miocene sedimentation in the Southern Taranaki Basin and implications for New Zealand plate boundary deformation. *Basin Research* **31**, 253–73.

Chemostrat Ltd (2017) Chemostratigraphy of six wells from the Kupe PML of the Manaia Graben, Southern Taranaki Basin, Offshore New Zealand. NZP&M Petroleum Report 5500, Wellington, New Zealand.

Clews P and Soo D (1994) Petrographic study of conventional core samples, well Maui BP-8. Core Laboratories. In MB-P(8) well completion report, Maui B Field, PML 381012, offshore Taranaki Basin (STOS, 1994). NZP&M Petroleum Report 2018, Wellington, New Zealand.

Coombs DS, Landis CA, Norris RJ, Sinton JM, Borns DJ and Craw D (1976) The Dun Mountain Ophiolite Belt, New Zealand its tectonic setting, constitution, and origin, with special reference to the southern portion. *American Journal of Science* **276**, 561–603.

Cooper RA (1989) Early Paleozoic terranes of New Zealand. *Journal of the Royal Society of New Zealand* **19**, 73–112.

Crampton J, Morgans H, Roncaglia L, Reid E, Schiøler P, Raine I and Fohrmann M (2012) *Quantitative Stratigraphy of Taranaki Basin.* GNS Science, Data Series 17A, Lower Hutt, New Zealand.

Crouch EM (2010) Palynology of the Turangi-3 and Kowhai-A1R wells, onshore Taranaki Basin. NZP&M Petroleum Report 5546, Wellington, New Zealand.

Crouch EM, Morgans HEG, Shepherd CL, Hollis CJ, Phillips A, Naafs BDA and Pancost RD (2020) Climatic and environmental changes across the Early Eocene Climatic Optimum at mid-Waipara River, Canterbury Basin, New Zealand. *Earth-Science Reviews* **200**, doi: 10.1016/j.earscirev.2019.102961.

Crouch EM and Raine JI (2012) Palynological study of the late Paleocene-early Eocene Kapuni Group section from four wells in the Kupe region, Taranaki Basin. NZP&M Petroleum Report 4574, Wellington, New Zealand.

Fedo CM, Nesbitt HW and Young GM (1995) Unraveling the effects of potassium metasomatism in sedimentary rocks and paleosols, with implications for paleoweathering conditions and provenance. *Geology* **23**, 921–24.

Fernández-Caliani JC, Galán E, Aparicio P, Miras A and Márquez MG (2010) Origin and geochemical evolution of the Nuevo Montecastelo kaolin deposit (Galicia, NW Spain). *Applied Clay Science* **49**, 91–7.

Folk RL, Andrews PB and Lewis DW (1970) Detrital sedimentary rock classification and nomenclature for use. *New Zealand Journal of Geology and Geophysics* **13**, 937–68.

Forster PM, Maycock AC, McKenna CM and Smith CJ (2020) Latest climate models confirm need for urgent mitigation. *Nature Climate Change* **10**, 7–10.

Garzanti E and Resentini A (2016) Provenance control on chemical indices of weathering. *Sedimentary Geology* **336**, 81–95.

Gradstein FM, Ogg JG, Schmitz MD and Ogg GM (eds) (2012) *The Geological Time Scale 2012*, Amsterdam: Elsevier, **2** vols, 1144 p.

Harnois L (1988) The CIW index: a new chemical index of weathering. *Sedimentary Geology* **55**, 319–22.

Higgs K (2002) Opito-1 petrographic study. NZP&M Petroleum Report 2710, Wellington, New Zealand.

Higgs K (2010) Petrology of the Kapuni Group in wells Kowhai-A1R and Turangi-3, Taranaki Basin. NZP&M Petroleum Report 4232, Wellington, New Zealand.

Higgs KE (2013) Mineralogical study of cuttings samples, Mauku-1, Taranaki Basin. NZP&M Petroleum Report 4859, Wellington, New Zealand.

Higgs K, Crouch E and Morgans H (2006) Turangi-1 well study. NZP&M Petroleum Report 4667, Wellington, New Zealand.

Higgs KE, Crouch EM and Raine JI (2017) An interdisciplinary approach to reservoir characterisation; an example from the early to middle Eocene Kaimiro Formation, Taranaki Basin, New Zealand. *Marine and Petroleum Geology* **86**, 111–39.

Higgs KE, Funnell RH and Reyes AG (2013) Changes in reservoir heterogeneity and quality as a response to high partial pressures of CO_2 in a gas reservoir, New Zealand. *Marine and Petroleum Geology* **48**, 293–322.

Higgs KE and King PR (2018) Sandstone provenance and sediment dispersal in a complex tectonic setting: Taranaki Basin, New Zealand. *Sedimentary Geology* **372**, 112–39.

Higgs KE, King PR, Raine JI, Sykes R, Browne GH, Crouch EM and Baur JR (2012a) Sequence stratigraphy and controls on reservoir sandstone distribution in an Eocene marginal marine-coastal plain fairway, Taranaki Basin, New Zealand. *Marine and Petroleum Geology* **32**, 110–37.

Higgs KE, Strogen D, Griffin A, Ilg B and Arnot M (2012b) Reservoirs of the Taranaki Basin, New Zealand. GNS Science, Data Series No. 2012/13a, Lower Hutt, New Zealand.

Higgs KE, Zwingmann H, Reyes AG and Funnell RH (2007) Diagenesis, porosity evolution, and petroleum emplacement in tight gas reservoirs, Taranaki Basin, New Zealand. *Journal of Sedimentary Research* **77**, 1003–25.

Hill PJ and Collen JD (1978) The Kapuni sandstones from Inglewood-1, Taranaki – petrology and effect of diagenesis on reservoir characteristics. *New Zealand Journal of Geology and Geophysics* **21**, 215–28.

Hollis CJ, Dunkley Jones T, Anagnostou E, Bijl P, Cramwinckel M, Edgar K and the DeepMIP project team (2019) The DeepMIP contribution to PMIP4: methodologies for selection, compilations and analysis of latest Paleocene and early Eocene climate proxy data, incorporating version 0.1 of the DeepMIP database. *Geoscientific Model Development Discussion* **2019**, 1–98.

Hollis CJ, Handley L, Crouch EM, Morgans HEG, Baker JA, Creech J, Collins KS, Gibbs SJ, Huber M, Schouten S, Zachos JC and Pancost RD (2009) Tropical sea temperatures in the high-latitude South Pacific during the Eocene. *Geology* **37**, 99–102.

Hornibrook N de B, Brazier R and Strong CP (1989) Manual of New Zealand Permian to Pleistocene foraminiferal biostratigraphy. *New Zealand Geological Survey Paleontological Bulletin* **56**, 175.

Howell DG (1980) Mesozoic accretion of exotic terranes along the New Zealand segment of Gondwanaland. *Geology* **8**, 487–91.

Ikhane PR, Akintola AI, Bankole SI, Ajibade OM and Edward OO (2014) Chemostratigraphic characterisation of siliciclastic rocks in parts of the Eastern Dahomey Basin, southwestern Nigeria. *Journal of Geography and Geology* **6**, 88–108.

Jarvis I and Jarvis KE (1992a) Inductively coupled plasma-atomic emission spectrometry in exploration geochemistry. In *Analytical Methods in Geochemical Exploration* (eds GEM Hall and B Vaughlin). *Journal of Geochemical Exploration* Special Issue **44**, 139–200.

Jarvis I and Jarvis KE (1992b) Plasma spectrometry in earth sciences: techniques, applications and future trends. In *Plasma Spectrometry in Earth Sciences* (eds I Jarvis and KE Jarvis). *Chemical Geology* **9**(1–2), 1–33.

Kamp PJJ (2012) Provenance study of northern Taranaki Eocene sediments. NZP&M Petroleum Report 4570, Wellington, New Zealand.

King PR, Naish TR, Browne GH, Field BD and Edbrooke SW (1999) *Cretaceous to Recent Sedimentary Patterns in New Zealand*. Institute of Geological & Nuclear Sciences, Folio Series 1, Lower Hutt, New Zealand, 35 p.

King PR and Thrasher GP (1992) Post-Eocene development of the Taranaki Basin, New Zealand; convergent overprint of a passive margin. In *Geology and Geophysics of Continental Margins* (eds JS Watkins, F Zhiqiang and KJ McMillen), pp. 93–118. American Association of Petroleum Engineers, Tulsa, Memoir **53**.

King PR and Thrasher GP (1996) Cretaceous-Cenozoic geology and petroleum systems of the Taranaki Basin, New Zealand. Institute of Geological & Nuclear Sciences, Monograph 13, Lower Hutt, New Zealand, 243 p.

Landis CA and Coombs DS (1967) Metamorphic belts and orogenesis in southern New Zealand. *Tectonophysics* **4**, 501–18.

Mange MA and Maurer HFW (1992) *Heavy Minerals in Colour*. London: Chapman & Hall, 147 p.

Martin KR, Baker JC, Hamilton PJ and Thrasher GP (1994) Diagenesis and reservoir quality of Paleocene sandstones in the Kupe South Field, Taranaki Basin, New Zealand. *American Association of Petroleum Geologists Bulletin* **78**, 624–43.

McCulloch MT, Bradshaw JY and Taylor SR (1987) Sm−Nd and Rb−Sr isotopic and geochemical systematics in Phanerozoic granulites from Fiordland, Southwest, New Zealand. *Contributions to Mineralogy and Petrology* **97**, 183–95.

McInerney FA and Wing SL (2011) The Paleocene-Eocene thermal maximum: a perturbation of carbon cycle, climate and biosphere with implications for the future. *Annual Review of Earth and Planetary Sciences* **39**, 489–516.

McLennan SM, Hemming SR, McDaniel DK and Hanson GN (1993) Geochemical approaches to sedimentation, provenance, and tectonics. In *Processes Controlling the Composition of Clastic Sediments* (eds MJ Johnsson and A Basu), pp. 21–40. Geological Society of America, Boulder, Special Paper 284.

Morgans HEG, Beu AG, Cooper RA, Crouch EM, Hollis CJ, Jones CM, Raine JI, Strong CP, Wilson GJ and Wilson GS (2004) Paleogene. In *The New Zealand Geological Timescale* (ed RA Cooper), Chapter 11. Institute of Geological & Nuclear Sciences, Lower Hutt, New Zealand, Monograph 22.

Mortimer N (2004) New Zealand's geological foundations. *Gondwana Research* **7**, 261–72.

Mortimer N, Rattenbury MS, King PR, Bland KJ, Barrell DJA, Bache F, Begg JG, Campbell HJ, Cox SC, Crampton JS, Edbrooke SW, Forsyth PJ, Johnston MR, Jongens R, Lee JM, Leonard GS, Raine JI, Skinner DNB, Timm C, Townsend DB, Tulloch AJ, Turnbull IM and Turnbull RE (2014) High-level stratigraphic scheme for New Zealand rocks. *New Zealand Journal of Geology and Geophysics* **57**, 402–19.

Mortimer N, Tulloch AJ and Ireland TR (1997) Basement geology of Taranaki and Wanganui Basins, New Zealand. *New Zealand Journal of Geology and Geophysics* **40**, 223–36.

Morton AC and Hallsworth CR (1999) Process controlling the composition of heavy mineral assemblages in sandstones. *Sedimentary Geology* **124**, 3–29.

Muir RJ, Ireland TR, Weaver SD, Bradshaw JD, Evans JA, Eby GN and Shelley D (1998) Geochronology and geochemistry of a Mesozoic magmatic arc system, Fiordland, New Zealand. *Journal of the Geological Society of London* **155**, 1037–53.

Muir RJ, Weaver SD, Bradshaw JD, Eby GN and Evans JA (1995) The Cretaceous Separation Point Batholith, New Zealand: granitoid magmas formed by melting of mafic lithosphere. *Journal of the Geological Society of London* **152**, 689–701.

Muir RJ, Weaver SD, Bradshaw JD, Eby GN, Evans JA and Ireland TR (1996) Geochemistry of the Karamea Batholith, New Zealand, and comparisons with the Lachlan Fold Belt granites of SE Australia. *Lithos* **39**, 1–20.

Murphy BH, Farley KA and Zachos JC (2010) An extraterrestrial ^{3}He-based timescale for the Paleocene-Eocene thermal maximum (PETM) from Walvis Ridge, IODP site 1266. *Geochimica et Cosmochimica Acta* **74**, 5098–108.

Nesbitt HW and Young GM (1982) Early Proterozoic climates and plate motions inferred from major element chemistry of lutites. *Nature* **299**, 715–7.

Parker A (1970) An index of weathering for silicate rocks. *Geological Magazine* **107**, 501–4.

Price RC, Spandler C, Arculus RJ and Reay AJ (2011) The Longwood Igneous Complex, Southland, New Zealand: A Permo-Jurassic, intra-oceanic, subduction-related, I-type batholithic complex. *Lithos* **126**, 1–21.

Raine JI (1984) Outline of a palynological zonation of Cretaceous to Paleogene terrestrial sediments in West Coast Region, South Island, New Zealand. New Zealand Geological Survey, Report 109, 82 p.

Raine JI (2004) New Eocene and Oligocene miospore zones and subzones. Appendix to Chapter 11. In *The New Zealand Geological Timescale* (ed RA Cooper), pp. 162–163. Institute of Geological & Nuclear Sciences, Lower Hutt, New Zealand, Monograph 22.

Raine JI, Beu AG, Boyes AF, Campbell HJ, Cooper RA, Crampton JS, Crundwell MP, Hollis CJ and Morgans HEG (2015) Revised calibration of the New Zealand Geological Timescale: NZGT2015/1. GNS Science, Lower Hutt, New Zealand, Science Report 2012/39, 53 p.

Raine JI and Mildenhall DC (2011) Palynological study of the upper Paleocene to Eocene interval in Kupe region wells, Taranaki Basin. NZP&M Petroleum Report 4377, Wellington, New Zealand.

Raine JI and Schiøler P (2012) Upper Cretaceous biostratigraphy of Maui-4 and Tane-1 wells, Taranaki Basin. GNS Science, Lower Hutt, New Zealand, Science Report 2012/28.

Rattenbury M, Cooper R and Johnston M (1998) (compilers) Geology of the Nelson Area: Lower Hutt, New Zealand. Institute of Geological & Nuclear Sciences, Lower Hutt, New Zealand, Geological Map 1:250,000 no. 9, 1 sheet and 67 p.

Roser BP, Coombs DS, Korsch RJ and Campbell JD (2002) Whole-rock geochemical variations and evolution of the arc-derived Murihiku Terrane, New Zealand. *Geological Magazine* **139**, 665–85.

Sagar MW, Palin JM, Tulloch AJ and Heath LA (2016) The geology, geochronology and affiliation of the Glenroy Complex and adjacent plutonic rocks, southeast Nelson. *New Zealand Journal of Geology and Geophysics* **59**, 213–35.

Smale D (1992) Provenance of sediments in Taranaki Basin – an assessment from heavy minerals. In *Petroleum Conference Proceedings 1*, pp. 245–254. Wellington: Ministry of Commerce.

Smale D (1996) Petrographic summaries of Taranaki petroleum reports: New Zealand. Institute of Geological and Nuclear Sciences, Lower Hutt, New Zealand, Science Report 96/1, 88 p.

Smale D, Maul JL, Palmer J, Soong R and Blattner P (1999) Variations in sandstone diagenesis with depth, time, and space, onshore Taranaki wells, New Zealand. *New Zealand Journal of Geology and Geophysics* **42**, 137–54.

Smale D and Morton AC (1987) Heavy mineral suites of core samples from the McKee Formation (Eocene-Lower Oligocene), Taranaki: implications for provenance and diagenesis. *New Zealand Journal of Geology and Geophysics* **30**, 299–306.

Smithies SL, Bassett KN, Browne GH and Nichols ARL (2019) Provenance of the Pakawau Group and Farewell Formation (Late Cretaceous–Paleocene), Taranaki Basin, northwest Nelson, New Zealand. *Zealand Journal of Geology and Geophysics*, published online 2 May 2019, doi: 10.1080/00288306.2019.1603164.

Sprague RA, Melvin JA, Conradi FG, Pearce TJ, Dix MA, Hill SD and Canham H (2009) Interogation of core-based chemostratigraphy and petrography of the Devonian Jauf Sandstones, Uthmaniya area, Ghawar Field, Eastern Saudi Arabia. *Search and Discovery*, Article 20065, 34.

Stagpoole V and Nicol A (2008) Regional structure and kinematic history of a large subduction back thrust: Taranaki Fault, New Zealand. *Journal of Geophysical Research* **113**, B01403. doi: 10.1029/2007JB005170.

STOS (1994) MB-P(8) well completion report, Maui B Field, PML 381012, offshore Taranaki Basin. NZP&M Petroleum Report 2018, Wellington, New Zealand.

Strogen DP (2011) Updated paleogeographic maps for the Taranaki Basin and surrounds. GNS Science, Lower Hutt, New Zealand, Science Report 2010/53, 83 p.

Strogen DP, Bland KJ, Nicol A and King PR (2014) Paleogeography of the Taranaki Basin region during the latest Eocene-Early Miocene and implications for the 'total drowning' of Zealandia. *New Zealand Journal of Geology and Geophysics* **57**, 110–27.

Strogen DP, Higgs KE, Griffin AG and Morgans HEG (2019) Late Eocene–Early Miocene facies and stratigraphic development, Taranaki Basin, New Zealand: the transition to plate boundary tectonics during regional transgression. *Geological Magazine* **156**(10), 1751–70.

Strogen DP, Seebeck H, Nicol A and King PR (2017) Two-phase Cretaceous–Paleocene rifting in the Taranaki Basin region, New Zealand; implications for Gondwana break-up. *Journal of the Geological Society* **174**, 929–46.

Thrasher GP (1990) Tectonics of the Taranaki rift. In *New Zealand Petroleum Conference Proceedings 1989*, pp. 124–133. Wellington: Ministry of Economic Development.

Tobin RC and Schwarzer D (2014) Effects of sandstone provenance on reservoir quality preservation in the deep subsurface: experimental modelling of deep water sand in the Gulf of Mexico. In *Provenance Studies in Hydrocarbon Exploration and Production* (eds RA Scott, HR Smyth, AC Morton and N Richardson), pp. 27–47. Geological Society of London, Special Publication no. 386.

Tulloch AJ (1983) Granitoid rocks of New Zealand – A brief review. *Geological Society of America, Memoir* **159**, 5–20.

Tulloch AJ (1988) Batholiths, plutons, and suites: nomenclature for granitoid rocks of Westland-Nelson, New Zealand. *New Zealand Journal of Geology and Geophysics* **31**, 505–9.

Tulloch AJ and Kimbrough DL (2003) Paired plutonic belts in convergent margins and the development of high Sr/Y magmatism: Peninsular Ranges batholith of Baja-California and Median batholith of New Zealand. In *Tectonic Evolution of Northwestern Mexico and The Southwestern USA* (eds S Johnson, S Patterson, J Fletcher, G Girty, D Kimbrough and A Martín-Barajas), pp. 275–95. Boulder, Colorado: Geological Society of America, Special Paper.

Tulloch AJ and Mortimer N (2017) New basement map of Taranaki Basin, New Zealand. In *Petroleum Geoscience Workshop*, Lower Hutt, New Zealand: GNS Science.

Tulloch AJ, Mortimer N, Ireland TR, Waight TE, Maas R, Palin JM, Sahoo T, Seebeck H, Sagar MW, Barrier A and Turnbull RE (2019) Reconnaissance basement geology and tectonics of South Zealandia. *Tectonics*, doi: 10.1029/2018TC005116.

Tulloch A and Palin M (2013) Provenance of detrital feldspar: Calibration of an LA-ICPMS trace element chemistry finger printing tool. GNS Science, Lower Hutt, New Zealand, Science Report 2012/35.

Tulloch AJ, Ramezani J, Kimbrough DL, Faure K and Allibone AH (2009) U–Pb geochronology and of mid-Paleozoic plutonism in western New Zealand: Implications for S-type granite generation and growth of the east Gondwana margin. *Geological Society of America Bulletin* **121**, 1236–61.

Vogel DE (1975) Precambrian weathering in acid metavolcanics rocks from the Superior Province. Villebon Township, south-central Quebec. *Canadian Journal of Earth Science* **12**, 2080–5.

Waight TE, Weaver SD, Muir JM, Mass R and Eby GN (1998) The Hohonu Batholith of North Westland, New Zealand: granitoid compositions controlled by source H_2O contents and generated during tectonic transition. *Contributions to Mineralogy and Petrology* **130**, 225–39.

Westerhold T, Röhl U, Donner B and Zachos JC (2018) Global extent of the Early Eocene hyperthermal events – a new Pacific benthic foraminiferal isotope record from Shatsky Rise (ODP site 1209). *Paleoceanography and Paleoclimatology*, doi: 10.1029/2017PA003306.

Worden RH, Mayall M and Evans IJ (2000) The effect of ductile-lithic sand grains and quartz cement on porosity and permeability in Oligocene and lower Miocene clastics, South China Sea: prediction of reservoir quality. *American Association of Petroleum Geologists Bulletin* **84**, 345–59.

Wright AM, Ratcliffe K, Bhattacharya J, Zhu Y and Wray DS (2010) The application of chemostratigraphy to fluvial-deltaic sequences: example from the Ferroan Sandstone Member, South-Central Utah. *Search and Discovery*, Article 40498, 55–60.

Zachos JC, Dickens GR and Zeebe RE (2008) An early Cenozoic perspective on greenhouse warming and carbon-cycle dynamics. *Nature* **451**, 279–83.

Zeebe RE, Ridgwell A and Zachos JC (2016) Anthropogenic carbon release rate unprecedented during the past 66 million years. *Nature Geoscience* **9**, 325–9.